

# **3-D Modeling Of Aerobic Biodegradation Of Petroleum Vapors: Effect Of Building Area Size On Oxygen Concentration Below The Slab**

U.S. Environmental Protection Agency  
Office of Underground Storage Tanks  
Washington, DC 20460

---

*[This page intentionally left blank.]*

---

**3-D Modeling Of Aerobic Biodegradation Of  
Petroleum Vapors: Effect Of Building Area Size On Oxygen  
Concentration Below The Slab**

Prepared by

Lilian Abreu, PhD.  
Arcadis U.S., Inc.  
100 Montgomery Street  
Suite 300  
San Francisco, CA 94104

Christopher C. Lutes  
Arcadis U.S., Inc.  
4915 Prospectus Drive  
Suite F  
Durham, NC 27713

and

Eric M. Nichols, P.E.  
Arcadis U.S., Inc.  
78 Piscassic Road  
Newfields, NH 03856

Contract No. GS-23F-0339K

for

U.S. Environmental Protection Agency  
Office of Underground Storage Tanks  
Washington, DC 20460

June 2013

---

*[This page intentionally left blank.]*

---

## **Disclaimer**

This document has been reviewed in accordance with U.S. Environmental Protection Agency policy and approved for publication. Mention of trade names or commercial products does not constitute endorsement or recommendation for use.

---

## **Acknowledgements**

Dr. Ian Hers and Dr. Parisa Jourabchi (Golder Associates, LTD); John A. Menatti (Utah Department of Environmental Quality) and Dr. Eric M. Suuberg (Brown University) provided technical peer reviews.

---

## Table of Contents

<b>Disclaimer .....</b>	<b>v</b>
<b>Acknowledgements .....</b>	<b>vi</b>
<b>List of Acronyms .....</b>	<b>x</b>
<b>Executive Summary .....</b>	<b>1</b>
<b>1. Introduction.....</b>	<b>1</b>
1.1 Background.....	1
1.2 Goal and Objectives.....	1
1.3 Document Development and EPA Peer Review.....	2
1.4 Document Organization.....	2
<b>2. Methodology .....</b>	<b>5</b>
2.1 Conceptualization of the Vapor Intrusion Process .....	5
2.2 Model Description .....	7
2.2.1 Model Capabilities .....	7
2.2.2 Model Limitations.....	8
2.3 Model Inputs .....	9
2.3.1 Building Footprint Size and Surrounding Land Cover .....	9
2.3.2 Source Depth and Concentration .....	11
2.3.3 Biodegradation Rate.....	12
2.3.4 Initial and Boundary Conditions for Petroleum Hydrocarbons and Oxygen.....	14
2.3.5 Chemical Composition of Vapor Source .....	14
2.3.6 Model Input Parameters .....	15
2.4 Sensitivity Testing .....	15
2.5 Potentially Confounding Factors .....	17
<b>3. Results and Discussion.....</b>	<b>19</b>
3.1 Summary of Tabulated Results.....	19
3.2 Graphical Conventions Used in Figures .....	19
3.3 Results for a Homogeneous Sandy Soil and Square Buildings .....	23
3.4 Results for a Homogeneous Sandy Soil and Rectangular Buildings .....	31
3.5 Results for a Homogeneous Sandy Soil with an Overlying Silty Clay Layer at Ground Surface .....	34
3.6 Results for Buildings with a Basement.....	36
<b>4. Conclusions.....</b>	<b>40</b>
<b>5. References .....</b>	<b>42</b>
<b>Appendix A. Model Equations</b>	
<b>Appendix B. Tabulated Simulation Results</b>	

---

## List of Tables

Table 1.	Theoretical Equivalent Units for Petroleum Hydrocarbon Vapor Concentrations Represented as Benzene. ....	12
Table 2.	Model Input Parameters .....	16

## List of Figures

Figure 1.	Large U.S. building (Boeing Facility, Everett, WA).....	10
Figure 2.	Comparison of biodegradation rates found in the literature.....	13
Figure 3.	Contours of simulated petroleum hydrocarbon vapors in the subsurface beneath a building. Results for PHC source vapor concentration of 10,000,000 $\mu\text{g}/\text{m}^3$ at depth of 15 ft (4.6 m) and building size of 2,073 ft x 2,073 ft (632 m x 632 m). Initial oxygen concentration of 21 percent by volume and transport time of 20 days. ....	20
Figure 4.	Contours of simulated oxygen concentrations in the subsurface beneath a building. Results for PHC source vapor concentration of 10,000,000 $\mu\text{g}/\text{m}^3$ at depth of 15 ft (4.6 m) and building size of 2,073 ft x 2,073 ft (632 m x 632 m). Initial oxygen concentration of 21 percent by volume and transport time of 20 days. ....	21
Figure 5.	Expanded view of portion of the 7 meter model domain outside the building footprint. Results for source vapor concentration of 10,000,000 $\mu\text{g}/\text{m}^3$ at depth of 15 ft (4.6 m) and building size of 2,073 ft x 2,073 ft (632 m x 632 m). Initial oxygen concentration of 21 percent by volume and transport time of 1 year. ....	22
Figure 6.	Concentration results for source vapor concentration of 10,000 $\mu\text{g}/\text{m}^3$ at depth of 5 ft (1.6 m) and building size of 2,073 ft x 2,073 ft (632 m x 632 m). Initial oxygen concentration of 21 and 10.5 percent by volume and transport time of 20 years. ....	24
Figure 7.	Concentration results for source vapor concentration of 100,000 $\mu\text{g}/\text{m}^3$ at depth of 5 ft (1.6 m) and building size of 2,073 ft x 2,073 ft (632 m x 632 m) over sandy soil. Initial oxygen concentration of 21 and 10.5 percent by volume and transport time of 20 years.....	25
Figure 8.	Concentration results for source vapor concentration of 1,000,000 $\mu\text{g}/\text{m}^3$ at depth of 5 ft (1.6 m) and building size of 2,073 ft x 2,073 ft (632 m x 632 m). Initial oxygen concentration of 21 percent by volume and transport times of 3, 6 and 9 years. ....	26
Figure 9.	Concentration results for source vapor concentration of 1,000,000 $\mu\text{g}/\text{m}^3$ at depth of 15 ft (4.6 m) and building size of 2,073 ft x 2,073 ft (632 m x 632 m) Initial	



---

oxygen concentration of 21 percent by volume and transport times of 6, 9 and 20 years. ....	27
Figure 10. Concentration results for source vapor concentration of 1,000,000 $\mu\text{g}/\text{m}^3$ at depth of 15 ft (4.6 m) and building size of 2,073 ft x 2,073 ft (632 m x 632 m) for an initial concentration of oxygen at 21% and 10% and transport times of 8 and 9 years. ....	28
Figure 11. Concentration results for source vapor concentration of 10,000,000 $\mu\text{g}/\text{m}^3$ at depth of 15 ft (4.6 m) and building size of 2,073 ft x 2,073 ft (632 m x 632 m) Initial oxygen concentration of 21 percent by volume. Three transport time: 20 days, 30 days and 1 year (steady state condition within one year of transport). ....	29
Figure 12. Concentration results for source vapor concentration of 10,000,000 $\mu\text{g}/\text{m}^3$ at depth of 15 ft (4.6 m) and three building sizes: 98 ft x 98 ft, 66 ft x 66 ft and 33 ft x 33 ft (30 m x 30 m, 20 m x 20 m, and 10 m x 10 m). Initial oxygen concentration of 21 percent by volume and steady state condition within one year of transport. ....	30
Figure 13. Concentration results for source vapor concentration of 10,000,000 $\mu\text{g}/\text{m}^3$ at depth of 30 ft (9 m) and three building sizes: 197 ft x 197 ft, 131 ft x 131 ft and 98 ft x 98 ft (60 m x 60 m, 40 m x 40 m, and 30 m x 30 m). Initial oxygen concentration of 21 percent by volume and steady state condition within one year of transport. ....	33
Figure 14. Concentration results for a building with rectangular shape 2073 ft x 33 ft (632 m x 10 m), source vapor concentration of 10,000,000 $\mu\text{g}/\text{m}^3$ at 15 ft (4.6 m), initial oxygen concentration of 21 percent by volume and steady state condition. Results viewed in two perpendicular cross sections by center of building. ....	35
Figure 15. Concentration results for building 2,073 ft x 2,073 ft (632 m x 632 m), with full 6.6 ft (2 m) deep basement, source vapor concentration of 100,000 $\mu\text{g}/\text{m}^3$ at 5 ft (1.6 m) below basement slab, transport time 9 years and initial oxygen concentration of 21 percent by volume. ....	37
Figure 16. Concentration results for building with full 2 m deep basement vs. building slab-on-grade, for building area 2,073 ft x 2,073 ft (632 m x 632 m), source vapor concentration of 100,000 $\mu\text{g}/\text{m}^3$ at 5 ft (1.6 m) below foundation slab, transport time 9 years and initial oxygen concentration of 21 percent by volume. ....	38

---

---

## List of Acronyms

bgs	Below ground surface
EPA	U.S. Environmental Protection Agency
$f_{oc}$	Mass fraction of organic carbon in soil
$K_{oc}$	Soil organic carbon
LNAPL	Light non-aqueous phase liquid
NAPL	Non-aqueous phase liquid
Pa	Pascal
PHC	Petroleum hydrocarbon
PVI	Petroleum vapor intrusion
psi	Pounds per square inch
USGS	United States Geological Survey
UST	Underground storage tank
VOC	Volatile organic compound

---

## **Executive Summary**

Vapor intrusion occurs when vapor-phase contaminants migrate from subsurface sources into buildings. One broad sub-category of vapor intrusion is petroleum vapor intrusion (PVI), in which vapors from petroleum hydrocarbons (PHCs) such as gasoline, diesel, or jet fuel enter a building. The intrusion of contaminant vapors into indoor spaces is of concern due to potential threats to safety (e.g., explosive concentrations of petroleum vapors or methane) and possible adverse health effects from inhalation exposure to toxic chemicals.

Petroleum vapors have the potential to attenuate in the subsurface as a result of microbially-mediated biodegradation. Aerobic biodegradation is typically the most significant process affecting the attenuation of petroleum vapors in the subsurface. Sufficient oxygen must be available beneath a building for rapid aerobic biodegradation of vapors from petroleum hydrocarbons (and other biodegradable volatile organic compounds) to occur and thereby reduce or eliminate the potential for PVI into overlying buildings.

The term oxygen shadow is qualitatively defined to mean existence of a concentration of oxygen at which the availability of oxygen substantially limits the rate of aerobic biodegradation. A generally accepted oxygen threshold in soil gas (and that which is used in this report) is 1 percent by volume (Winegardener and Testa, 2002; Abreu and Johnson, 2006; Abreu et al., 2009a; Ward, 1997; Davis, 2009).

### **ES.1 Purpose and Document Focus**

The purpose of this technical document is to report on 3-D finite difference vapor transport modeling simulations designed to systematically assess the development of an oxygen shadow beneath a building. These new simulation results are aimed at improving the understanding of the impact of building footprint size on the oxygen shadow and will help to inform development of guidance on petroleum vapor intrusion by the U.S. Environmental Protection Agency's (EPA) Office of Underground Storage Tanks. These scenarios extend the simulations presented in Abreu and Johnson (2005, 2006); Abreu et al. (2009a,b); and U.S. EPA (2012).

### **ES.2 Methodology**

The work presented in this technical document features three-dimensional (3-D) mathematical model simulations for a range of building sizes, source concentrations, and depths. The 3-D model used in this work was developed by Abreu and Johnson (2005, 2006). Starting from a base case model simulation, subsequent simulations were conducted to determine whether there are size thresholds above which an oxygen shadow is always present, and below which an oxygen shadow does not develop. Subsequent simulations were chosen based on the results of these initial simulations and decreasing or increasing the building size. All other parameters were reasonably representative of typical conditions and were held constant during the modeling simulations. Soil properties for the base cases were for a homogeneous sandy soil and the simulation was run for various durations to determine if quasi-steady state conditions had been achieved or to verify the length of time before oxygen is depleted by aerobic biodegradation and

---

an oxygen shadow develops. Additional scenarios were run for a sandy soil overlain by a one meter silty clay layer.

For the approximately 160 simulations in this report, only factors easily identified in the site screening process (e.g., foundation dimensions and thickness of the vadose zone) were considered. It is likely that results would change significantly if additional processes (e.g., high permeability layers beneath building slabs, wind speed/direction variability and bi-directional flow through foundation cracks and penetrations throughout the floor plan) were modeled.

### **ES.3 Findings and Conclusions**

The results of this study may help practitioners identify situations where they should confirm with field measurements the presence of oxygen necessary to support aerobic biodegradation of petroleum hydrocarbons. Conversely, there are other situations where practitioners can reasonably infer from site conditions the presence of a sufficient level of oxygen.

Simulation results indicate that the probability of an oxygen shadow developing increases with:

- Increasing building area (including surrounding pavement area)
- Increasing source vapor concentration
- Decreasing depth of vapor source beneath the building
- Increasing transport time for oxygen consumption under transient conditions (assuming the source PHC vapor concentrations are stable)

---

# 1. Introduction

## 1.1 Background

Vapor intrusion occurs when vapor-phase contaminants migrate from subsurface sources into buildings. Petroleum vapor intrusion (PVI) occurs when vapors from petroleum hydrocarbons such as gasoline, diesel, or jet fuel enter a building. The intrusion of contaminant vapors into indoor spaces is of concern due to potential threats to safety (e.g., explosive concentrations of petroleum vapors or methane) and possible adverse health effects from inhalation exposure to toxic chemicals.

Petroleum vapors have the potential to attenuate in the subsurface as a result of microbially-mediated biodegradation. Aerobic biodegradation is typically the most significant process affecting the attenuation of petroleum vapors in the subsurface. Sufficient oxygen must be available beneath a building to support biodegradation of vapors from petroleum hydrocarbons and other biodegradable volatile organic compounds (VOCs) and thus decrease or eliminate the potential for PVI into overlying buildings.

Preliminary modeling results (Abreu et al., 2009; Abreu and Johnson, 2005, 2006) indicate that beneath buildings and other lower permeability ground covers, soil vapor may become depleted of oxygen, forming an oxygen shadow. The term oxygen shadow refers to a concentration of oxygen at which its availability substantially limits the rate of aerobic biodegradation. A generally accepted oxygen threshold in soil gas used in this report is 1 percent by volume (Winegardener and Testa, 2002; Abreu and Johnson, 2006; Abreu et al., 2009a; Ward, 1997; Davis, 2009). Where an oxygen shadow occurs, the potential for PVI into buildings is increased. This oxygen shadow is the result of an interrelationship among several factors including the following:

- Building footprint
- Source concentration
- Depth of contamination
- Length of time for vapor and oxygen transport
- Underlying soil types and stratification

## 1.2 Goal and Objectives

The goal of this study was to determine whether there is a threshold building footprint size, above which a permanent oxygen shadow may form beneath the center of an overlying building. This was to be accomplished by using a 3-D mathematical model to simulate development of an oxygen shadow beneath buildings of various sizes. These simulations expand upon those presented in Abreu and Johnson (2005, 2006), Abreu et al. (2009a,b), and U.S.EPA (2012). This report was prepared in support of EPA's *Guidance For Addressing Petroleum Vapor Intrusion At Leaking Underground Storage Tank Sites*.

---

### **1.3 Document Development and EPA Peer Review**

A draft of the document was subjected to EPA's external peer review process from May to June 2012. The peer review contractor independently selected four experts not affiliated with EPA. Dr. Ian Hers and Dr. Parisa Jourabchi (Golder Associates, LTD); John A. Menatti (Utah Department of Environmental Quality) and Dr. Eric M. Suuberg (Brown University) provided technical peer reviews. The expertise of the peer review panel includes:

- Practical and theoretical understanding of the petroleum vapor intrusion pathway, including how volatile organic contaminants move and distribute in the subsurface (soil gas), indoor air, and outdoor air from dissolved and nonaqueous phase liquid sources
- Experience in planning and conducting site-specific vapor intrusion studies, including developing and refining conceptual site models of the migration and distribution of volatile contaminants
- Expertise in 3-D numerical modeling of vapor intrusion processes, applying and calibrating models using site-specific data, and interpreting results to make decisions at vapor intrusion sites

The peer reviewers were tasked to review the draft report and provide opinion and perspective regarding the following:

- Whether the model and model runs are suitable and sufficient for the objectives of the investigation
- The scientific appropriateness of using results from a numerical model for developing screening criteria based on the dimensions of a building given the wide possibilities for the foot print of a building that might be impacted by PVI, and given the relatively limited empirical literature relating the dimensions of a building to the possibility for vapor intrusion
- Whether the model inputs are reasonably representative of worst-case conditions for oxygen depletion in the vadose zone immediately underlying a building
- Whether the reported conclusions are adequately supported by the simulation results

The document was then revised to address the comments of the peer reviewers. Additional revisions to the final draft were made by EPA to conform to formatting standards.

### **1.4 Document Organization**

This report is organized as follows:

- Section 2 – Methodology
- Section 3 – Results and Discussion

- 
- Section 4 – Conclusions
  - Section 5 – References

---

*[This page intentionally left blank.]*



---

## 2. Methodology

### 2.1 Conceptualization of the Vapor Intrusion Process

Vapor intrusion occurs when VOCs from contaminated soils or groundwater migrate upwards toward the ground surface and into overlying buildings through gaps and cracks in foundation slabs or basement walls. This contaminant migration is driven by differences in concentrations and air pressure between the contaminated subsurface regions and the affected buildings. The vapor intrusion pathway is the route VOCs take from a source through the subsurface and eventually intrude into a building. Entry routes into the building must exist for the vapors to enter the building and driving forces must exist to cause the vapors to enter the building for the pathway to be complete (U.S. EPA, 2012).

Some VOCs, especially petroleum hydrocarbon (PHC) vapors, readily biodegrade when sufficient oxygen is present in soil gas. Biodegradation reduces the concentrations of PHCs in soil gas as they migrate through the soil from the contaminant source into indoor air. This reduction in concentration from a measurement point in the subsurface to indoor air is referred to as attenuation. The extent of attenuation depends on the source concentration, the amount of oxygen available for biodegradation, the biodegradation rate, soil moisture content, and the length of time for vapor/gas transport (which is a function of the length of the transport pathway). Subsurface transport of PHC vapors can be affected by the following:

- Subsurface features (e.g., fine-grained soils, soils with high-moisture content) that may hinder the diffusion and advection of VOCs
- Biodegradation of contaminants
- Presence of entry routes through the building foundation and sub-grade walls
- Changes with time in groundwater level, source strength, and infiltration rates
- Pressurization of the building (under-pressurization draws soil gas into a building)
- Air exchange into a building, which brings fresh air into the enclosed space and dilutes the concentration of VOCs that enter through the vapor intrusion pathway (EPA, 2012)

Sources of subsurface PHC vapors include leaking gas pipes, leaking underground storage tanks (USTs), aboveground spills, aboveground facilities that use PHCs during operations, historical subsurface disposal of industrial wastes, and landfills. At leaking UST sites, the primary contaminants of concern are petroleum fuels such as gasoline and diesel. When these substances are released into the subsurface, they may partition into several phases:

- Residual phase non-aqueous phase liquid (NAPL) occurring as disconnected globules trapped within soil pore spaces
- Mobile phase NAPL (i.e., free product)
- Aqueous phase dissolved in soil moisture and groundwater

- 
- Vapor phase in soil gas

NAPL masses comprised of substances less dense than water are light NAPLs or LNAPLs. LNAPL sources are of particular concern because they typically create higher vapor concentrations in soil gas and potentially greater mass flux than do dissolved groundwater plumes containing the same chemicals. The simulations in this technical document assume a vapor source in soil gas above the groundwater table; the vapors may originate from either dissolved VOCs in groundwater at the top of the capillary fringe or LNAPL (residual or mobile) accumulations near the water table.

Vapor transport in the subsurface may be controlled by four primary processes:

- Diffusion occurs when there are spatial differences in VOC concentrations in the subsurface; vapors diffuse in the direction of lower concentrations.
- Advection occurs when there is bulk movement of soil gas induced by spatial differences in soil gas pressure.
- Phase partitioning refers to the processes leading to VOC distribution between the soil gas, the dissolved phase in soil pore water, and the sorbed phase on soil particle surfaces. Phase partitioning will retard contaminant vapor transport in the subsurface under transient conditions, but not under steady-state transport conditions, when the mass transfer between phases approaches equilibrium.
- Degradation is usually associated with biodegradation, in which VOCs are converted to other chemicals by microorganisms in the subsurface.

Vapor transport may occur under transient or steady state conditions. Under transient conditions, concentrations are changing with time. Under steady state conditions, concentrations and pressures are constant with time, although they may vary spatially. Under steady state conditions, the parameters that influence transport by diffusion and advection:

- Soil porosity and moisture content
- Chemical diffusion coefficients in air and water
- Soil gas permeability
- Building pressurization relative to adjacent soil gas pressures

The Henry's law constant (which quantifies chemical partitioning between air and water) may also influence transport when moisture content is high and Henry's law constant is very low. For transient transport conditions, VOC transport may also be influenced by phase transfer to the aqueous and solid phases, which depend on the VOC-specific Henry's law constant and sorption coefficient to soil organic carbon ( $K_{oc}$ ), and on the mass fraction of organic carbon in soil ( $f_{oc}$ ) (EPA, 2012).

---

## 2.2 Model Description

### 2.2.1 Model Capabilities

The vapor intrusion model developed by Abreu and Johnson (2005, 2006) and used during this study is a three-dimensional, finite difference model. The Abreu-Johnson 3-D model (the 3-D model) simultaneously solves transient transport equations (Appendix A) for the following:

- Soil-gas pressure field (from which the advective flow field is computed)
- Transient advective and diffusive transport and reaction of multiple chemicals (including oxygen) in the subsurface
- Flow and chemical transport through foundation cracks
- Chemical mixing in indoor air

Starting from a base case comprised of a homogeneous sandy soil and a building of 33 ft x 33 ft (10 m x 10 m), a series of model simulations were conducted by varying the building size and geometry, source concentration, depth to the source, transport time, and initial oxygen concentration. All other parameters were reasonably representative of typical conditions and were held constant during the modeling simulations.

Although the model has the capability of simulating heterogeneous soil moisture distributions beneath and adjacent to a building, formation of a moisture shadow<sup>1</sup> beneath buildings (or the increased infiltration of rain water below a roof's drip edge) was not simulated.

The soil gas concentration distribution in the subsurface is symmetrical to the center of the building in the x and y dimensions for all scenarios simulated in this document. For computational efficiency the model domain was set up to take advantage of this symmetry by simulating vapor transport using only ¼ of the building footprint. For example, for a 33 ft x 295 ft (10 m x 90 m) building, only ¼ of its footprint area 15 ft x 148 ft (5 m x 45 m) is input into the 3-D model domain.

The numerical accuracy of the 3-D model has been previously demonstrated through the comparison of model predictions with other analytical and numerical model results. The 3-D model has been shown to be capable of fitting field measured vertical soil gas profiles. These results are discussed in Abreu et al. (2009a,b and 2007) and Abreu and Johnson (2005, 2006).

The majority of the simulations presented in this report represent quasi-steady state transport conditions; only a few transient transport scenarios are illustrated and discussed. Because the 3-D model is a transient solution of the transport equations, the steady state scenarios presented in this document were obtained by running simulations over a time period of sufficient length to effectively represent steady state conditions (EPA, 2012). Verification that steady state conditions had been reached was achieved by the following:

---

<sup>1</sup> Soil moisture contents of 25 percent to 85 percent of field capacity are considered necessary for biodegradation to occur in vadose zone soil (Ward, 1997).

- 
- Running the scenario for a given period of transport time
  - Re-running the scenario for a longer transport time
  - Comparing results of the two simulations to check whether additional simulation time resulted in significant changes in concentration distribution in the subsurface or in the indoor air concentration. If no significant changes were observed, it was assumed that a quasi-steady state condition had been achieved.

### **2.2.2 Model Limitations**

The 3-D model simulates the transport of contaminant vapors in the unsaturated soil zone; it does not model the transport of dissolved contaminants via groundwater flow in the saturated zone.

The foundation floor and walls are simulated as impermeable barriers to the transport of vapors from the subsurface to the indoors, except where there are cracks or openings in the foundation. The baseline conditions for most simulations presented in this document assume:

- Slab-on-grade building
- Full-length perimeter crack shown in figure A-1 of Appendix A
- Building with a steady under-pressurization of  $7.3 \times 10^{-4}$  psi (5 Pa)
- Relatively dry sandy soils
- Constant source concentration (i.e., no depletion of the source), and
- Infinite source footprint area covering the full extent of the building slab and beyond

The 3-D model simulates buildings with basement or slab-on-grade foundations; it does not simulate buildings with a crawl space.

In actual foundations, the ability of concrete to transmit soil gas depends on the physical integrity of the concrete and characteristics determined by cement mixtures, cement/water ratios, and production processes (e.g., poured concrete vs. concrete block). Intact concrete is virtually impermeable to advective air flow; however, in real settings volatile compounds from soil gas may diffuse through a concrete slab and oxygen may also diffuse from indoor air toward soil gas through a concrete slab.

In a site assessment for vapor intrusion, any relevant background VOC levels (i.e., contaminants in indoor air that come from either indoor sources or from outdoor air) should be taken into consideration. As a simplifying assumption, all VOCs in indoor air are the result of vapor intrusion and that there are no background VOC contributions from either indoor or outdoor sources. In addition, indoor air concentrations are assumed to be uninfluenced by sorption (or desorption) to building materials (U.S EPA, 2012).

---

## 2.3 Model Inputs

Inputs to the model include:

- Geometry descriptors (e.g., building footprint, foundation depth, crack locations and widths, source depth, source footprint)
- Chemical properties
- Kinetic reaction rate parameters
- Indoor-outdoor pressure differential
- Oxygen concentration at the ground surface
- Chemical vapor concentrations at the vapor source

### **2.3.1 Building Footprint Size and Surrounding Land Cover**

The goal of this study was to determine whether there is a threshold building footprint size, above which a permanent oxygen shadow may form beneath the center of an overlying building. This was to be accomplished by using a 3-D model to simulate development of an oxygen shadow beneath buildings of various sizes. Building size parameters were selected based on a review of published information. According to Census Bureau data from 2007, the majority of the new single-family housing units sold in the U.S. between 1999 and 2007 have a floor area that ranges between 1,000 and 5,000 ft<sup>2</sup> (93 to 464 m<sup>2</sup>). Koomey (1990) reports the size distribution of commercial buildings:

- 55 percent are from 1,001 to 5,000 ft<sup>2</sup> (93 to 464 m<sup>2</sup>)
- 22 percent are from 5,001 to 10,000 ft<sup>2</sup> (464 to 927 m<sup>2</sup>)
- 12 percent are from 10,001 to 25,000 ft<sup>2</sup> (927 to 2,318 m<sup>2</sup>)
- 5.7 percent are from 25,001 to 50,000 ft<sup>2</sup> (2,318 to 4,636 m<sup>2</sup>)

Starting from a base case model run (a square building 33 x 33 ft [10 x 10 m] overlying sandy soil), a series of simulations were conducted to determine the building size threshold. The first set of simulations used a building size of 295 ft x 295 ft (90 m x 90 m); a size chosen to reasonably include building sizes within the distribution found in the USA. The largest footprint modeled was a building with a footprint of 4.3 million ft<sup>2</sup> (2,073 ft x 2,073 ft or 632 m x 632 m). Figure 1 presents a photograph of a building of this size. Approximately 160 simulations were conducted; the results are tabulated in Tables B-1 through B-5 in Appendix B.

In addition to reported building floor plan sizes, many U.S. buildings are surrounded by parking lots, driveways, sidewalks, or roads. If the buildings and surrounding areas are in good condition and not broken up by a significant number of cracks or expansion joints, they may extend the effective footprint area subject to formation of an oxygen shadow. Parking lots separated from buildings by planting beds and asphalt parking lots are less likely to contribute to



**Figure 1. Large U.S. building (Boeing Facility, Everett, WA). Image downloaded from [http://www.boeing.com/commercial/tours/images/K64532-14\\_lg.jpg](http://www.boeing.com/commercial/tours/images/K64532-14_lg.jpg).**

the formation of an oxygen shadow. Most asphalt pavements should have a permeability similar to the hydraulic conductivity of fine silty sand (Shan, undated).

Subsurface vapor flow may differ for equal footprint sizes (smaller building surrounded by a concrete parking lot equals the footprint of a larger building) due to the depressurization of the interior space (assumed 5 Pa in these simulations). The air permeability of concrete increases gradually with time, reaching a nearly stable value after 20 years that is similar to the permeability of homogeneous clay (Nazaroff, 1988). The air permeability of soils modeled in this study is greater than that of concrete.

The 3-D modeling simulations conducted by U.S. EPA (2012) used a 33 ft x 33 ft (10 m x 10 m) square building. In a square building overlying a homogeneous and isotropic soil, oxygen transport to the center of the building footprint would occur uniformly from all four directions. It is reasonable to expect that in the case of a rectangular building, the magnitude of oxygen transport along the long axis of the building would be lower relative to oxygen transport along the short axis. Therefore, the simulations in Tables B-1 through B-5 (Appendix B), include some rectangular cases.

---


### **2.3.2 Source Depth and Concentration**

Simulations were repeated for three source depths: 5, 15 and 30 ft (1.6, 4.6, and 9 m, respectively), and source vapor concentrations in the range of 10,000  $\mu\text{g}/\text{m}^3$  to 10,000,000  $\mu\text{g}/\text{m}^3$ . In some cases, as many as six source vapor concentration increments were simulated: 10,000  $\mu\text{g}/\text{m}^3$ , 100,000  $\mu\text{g}/\text{m}^3$ , 1,000,000  $\mu\text{g}/\text{m}^3$ , 2,000,000  $\mu\text{g}/\text{m}^3$ , 5,000,000  $\mu\text{g}/\text{m}^3$  and 10,000,000  $\mu\text{g}/\text{m}^3$  in the soil vapor phase. This source strength range is reasonable for simulating releases of petroleum fuels from leaking USTs because:

- Concentrations less than 10,000  $\mu\text{g}/\text{m}^3$  are very unlikely to exhibit an oxygen shadow regardless of what values were selected for the other model parameters (see Section 2.3.6).
- EPA (2012, Section 5) presents results for scenarios using source strengths from 20,000,000  $\mu\text{g}/\text{m}^3$  through 200,000,000  $\mu\text{g}/\text{m}^3$  for a 33 ft x 33 ft (10 m x 10 m) building. These results showed some instances where oxygen was depleted even for such a relatively small building size. Abreu et al. (2009b) presents simulation results using the same 3-D model and building size for source strengths of 4,000  $\mu\text{g}/\text{m}^3$ , 40,000  $\mu\text{g}/\text{m}^3$ , 400,000  $\mu\text{g}/\text{m}^3$ , 1,000,000  $\mu\text{g}/\text{m}^3$ , 4,000,000  $\mu\text{g}/\text{m}^3$ , 10,000,000  $\mu\text{g}/\text{m}^3$ , 40,000,000  $\mu\text{g}/\text{m}^3$ , 100,000,000  $\mu\text{g}/\text{m}^3$ , 200,000,000  $\mu\text{g}/\text{m}^3$  and 400,000,000  $\mu\text{g}/\text{m}^3$ .
- Published estimates of soil gas concentrations in equilibrium with gasoline LNAPL range from 220,000,000  $\mu\text{g}/\text{m}^3$  (220 mg/L) for weathered gasoline to 1,300,000,000  $\mu\text{g}/\text{m}^3$  (1,300 mg/L) for fresh gasoline (Johnson et al., 1990).
- The simulated range of source vapor concentrations corresponds approximately to a range dissolved phase hydrocarbon concentrations from 0.01 mg/L to 10 mg/L, which is a typical range for groundwater concentrations in equilibrium with older releases of petroleum LNAPL (Lahvis et al., 2013; U.S. EPA, 2013).
- According to EPA (2012, p.66): “A hydrocarbon vapor source concentration of 20,000 mg/m<sup>3</sup> (20,000,000  $\mu\text{g}/\text{m}^3$ ) might be encountered at sites where the vapor source is gasoline or hydrocarbons dissolved in groundwater. A source vapor concentration of 200,000 mg/m<sup>3</sup> (200,000,000  $\mu\text{g}/\text{m}^3$ ) might be encountered at sites where the source is weathered gasoline NAPL just above the water table.”

The information in the preceding bullets is summarized in Table 1 to facilitate interpretation of the magnitude of the vapor source concentrations used as input values in the 3-D model.

**Table 1. Theoretical Equivalent Units for Petroleum Hydrocarbon Vapor Concentrations Represented as Benzene.**

Liquid (Approximate Equivalent)		Vapor $\mu\text{g}/\text{m}^3$	Type of Vapor Source
mg/L	$\mu\text{g}/\text{L}$		
0.01	10	10,000	
0.1	100	100,000	
1.0	1,000	1,000,000	
10.0	10,000	10,000,000*	
220	220,000	220,000,000	
1,300	1,300,000	1,300,000,000	
*highest concentration simulated in the present study			

### **2.3.3 Biodegradation Rate**

The simulations reported here employ a first-order biodegradation model with a biodegradation rate ( $\lambda$ ) of  $0.79 \text{ h}^{-1}$  for aromatic hydrocarbons, which is consistent with Abreu et al. (2009a, b) and within the midrange of reasonably accepted values. This biodegradation rate is the average reported for aromatic hydrocarbons in the analysis of DeVaul (2007), who compiled results from 84 data sets of laboratory and field biodegradation rates for aromatic hydrocarbons measured by multiple investigators. Figure 2 illustrates how the selected biodegradation rate relates to other biodegradation rates that were tested in previous studies, which are summarized later in this section. This biodegradation rate can also be compared to the values of  $0.48 \text{ h}^{-1}$  for aromatic hydrocarbons summarized by DeVaul (2011). The sensitivity of the results of the 3-D model to various biodegradation rates is presented in Abreu and Johnson (2006) and Abreu et al. (2009a,b).

Abreu et al. (2009b, pp.13-14) published additional simulations showing the oxygen distribution at three somewhat different biodegradation rates ( $0.079 \text{ h}^{-1}$ ,  $0.79 \text{ h}^{-1}$  and  $2 \text{ h}^{-1}$ ). They examined slab-on-grade and basement scenarios with a  $4,000,000 \mu\text{g}/\text{m}^3$  vapor source at 13.2 ft (4 m) bgs (a substantially lower concentration range than used in Abreu and Johnson [2006]). For these lower source strengths, varying the biodegradation rate from  $0.079 \text{ h}^{-1}$  to  $0.79 \text{ h}^{-1}$  did not affect the formation of an oxygen shadow. Ample oxygen is available for biodegradation under these conditions, though subsurface oxygen concentrations decrease as  $\lambda$  increases due to increasing rates of oxygen utilization. The sensitivity of the modeled biodegradation in the 3-D model to various biodegradation rates under various conditions of source concentration is shown as Figures 30, 31, 33, 34 and 36 in U.S. EPA (2012) and Figures 5, 6, 12 and 13 in Abreu et al. (2009b).

Biodegradation rates for aromatic hydrocarbons are not directly comparable to those for aliphatic hydrocarbons. However, the ratio of oxygen to hydrocarbon consumed is typical of the stoichiometric ratio for the complete mineralization of hydrocarbons to carbon dioxide (i.e., 3 kg-oxygen per 1 kg-hydrocarbon). More discussion of this is presented in Section 2.3.5.



Simulations using individual properties of aromatic and aliphatic hydrocarbons with their respective biodegradation rates show that oxygen consumption is equivalent, regardless of the mixture of petroleum compounds being simulated as long as the total vapor concentration of the source is the same (Abreu et al., 2009b).

Simulations published by Abreu and Johnson (2006, pp. 2309-2310) show the oxygen distribution for three biodegradation rates (0.018, 0.18 and 1.8 h<sup>-1</sup>) slab-on-grade and basement scenarios with 200,000,000 µg/m<sup>3</sup> vapor source strength at 16.5 ft (5 m) below ground surface (bgs). In general, these results show that for high source concentrations (e.g., 200,000,000 µg/m<sup>3</sup>) and depths of 16.5 ft (5 m) or less the biodegradation rate doesn't significantly affect the size of the oxygen shadow. In these cases the simulated oxygen shadow extends across virtually the entire building footprint regardless of the biodegradation rate selected (Abreu and Johnson, 2006). For these simulations, the observed oxygen penetration depth of about 8.25 ft (2.5 m) bgs appeared to be relatively unaffected by first-order degradation rate for this source concentration and depth. For all three degradation rates, simulated steady state soil gas profiles near the foundation were influenced by the presence of the foundation for both basement and slab-on-grade scenarios. In these simulations, oxygen is not present beneath the foundation at normalized

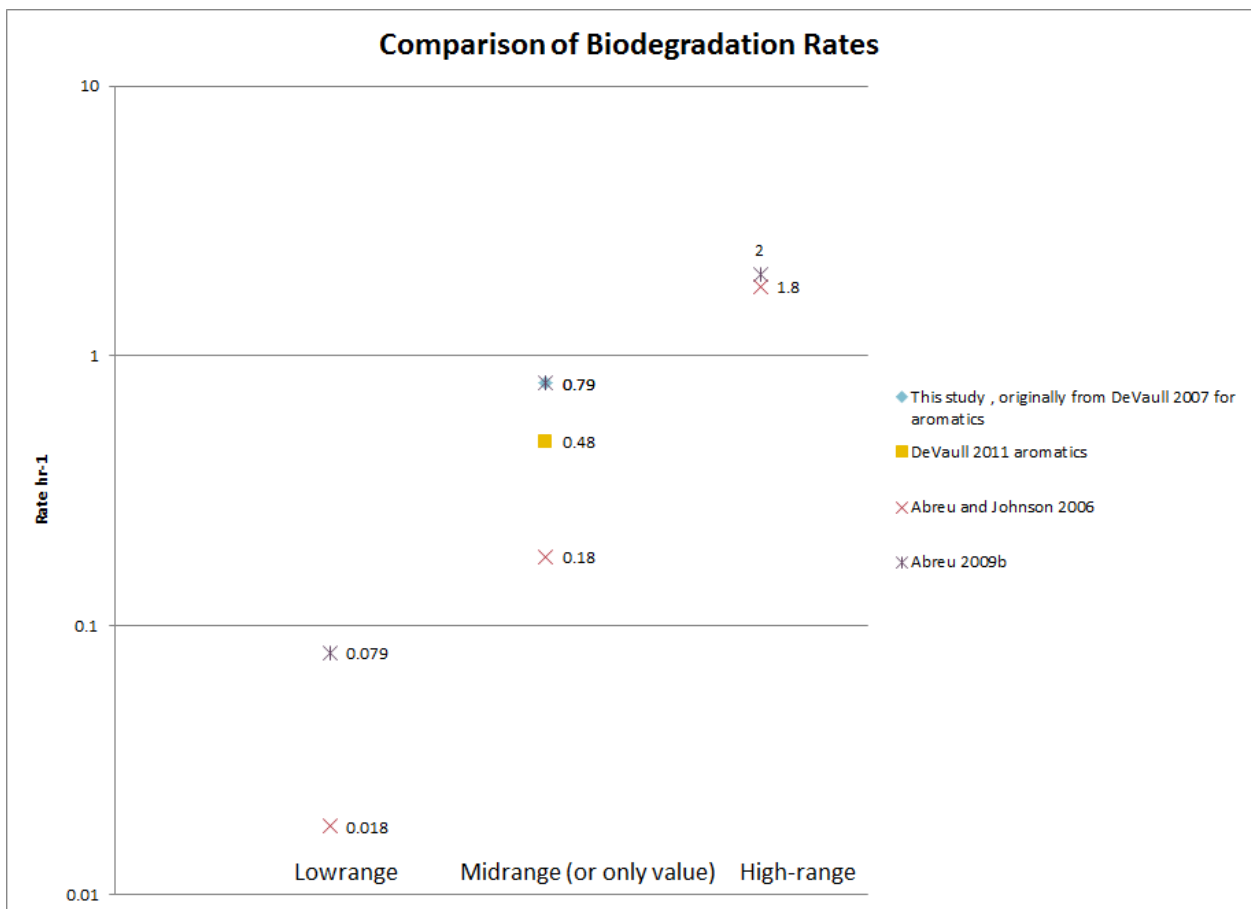


Figure 2. Comparison of biodegradation rates found in the literature.

---

concentrations  $>0.05$ . Thus, these scenarios indicate that hydrocarbon vapor concentrations are relatively unaffected by changes in first-order biodegradation rate when insufficient oxygen concentrations exist beneath a foundation to support aerobic degradation.

From all of the simulations described in the preceding paragraphs, it is observed that for high source strengths and low oxygen levels, soil gas concentration profiles for PHCs and oxygen are insensitive to biodegradation rates. Conversely, for low source strengths and higher oxygen levels, PHC vapor and oxygen concentration profiles are sensitive to biodegradation rates. Specifically, in order for the biodegradation rate to influence development of an oxygen shadow below a building, two conditions must be met:

- Oxygen concentration in soil gas must not be less than 2 percent by volume (i.e., there must be sufficient oxygen available to support biodegradation), and
- Biodegradation rate must be greater than  $2 \text{ h}^{-1}$ , which is in the high range of reported values (see Figure 2) and higher than the values used in the studies discussed in this section.

#### **2.3.4 Initial and Boundary Conditions for Petroleum Hydrocarbons and Oxygen**

The 3-D model was used to simulate the coupled transport and biodegradation of PHCs and oxygen. The PHC source is assumed to be constant concentration and infinite extent located at the lower boundary of the domain. At the upper boundary, the atmosphere is simulated as a constant source of oxygen at 21 percent by volume. The oxygen influx is through the open ground surface area next to the building. The initial concentration of oxygen in the subsurface was assumed to be 21 percent by volume (the same as the atmospheric concentration). For some simulations, the initial oxygen concentration in the subsurface was reduced to 10.5 percent by volume; half of the oxygen concentration in the influx from the atmosphere at the open ground (see Section 2.4 for more discussion).

In all simulations, the threshold oxygen concentration for biodegradation to occur was assumed to be 1 percent by volume (which corresponds to a normalized oxygen concentration of 0.05 in the contour plots) (Abreu and Johnson, 2006; Abreu et al., 2009a,b; Ward et al., 1997; Patterson and Davis, 2009).

#### **2.3.5 Chemical Composition of Vapor Source**

Aerobically biodegradable chemicals (such as PHCs) simultaneously utilize oxygen and thus, contribute to its depletion in the subsurface. Benzene is typically used as a surrogate for all aerobically biodegradable PHCs and other VOCs of interest for PVI investigations.<sup>2</sup> All simulations presented in this report assume a single-component vapor source with physical-

---

<sup>2</sup> When applying the results of this study to other sites, an equivalent benzene concentration should be calculated for all degradable VOCs (i.e. total petroleum hydrocarbons plus methane) and the result used as the source vapor concentration. Likewise, the biodegradation rate and other physical and chemical properties for benzene should be used as model inputs.

---

chemical properties for benzene. Abreu et al. (2009a,b) compared predicted VOC concentrations and oxygen profiles for cases involving single and multicomponent sources with the same total source concentration. For cases where oxygen is limiting and biodegradation rates are variable (but fast compared with diffusive transport time scales), the vapor profiles of individual components were similar. This behavior has been observed in the field and documented by Roggemans et al. (2001). Abreu et al. (2009a,b) present simulation results using a higher biodegradation rate of  $71 \text{ hr}^{-1}$  for aliphatic hydrocarbons. However, very similar oxygen profiles were observed with the single-source benzene and multicomponent petroleum hydrocarbon cases. Therefore, while the simulations presented in this report are for a single component source, they are also applicable to a range of multicomponent sources involving aerobically biodegradable chemicals (EPA, 2012).

As discussed in Section 3, for certain source concentrations and depths, the oxygen concentrations in the subsurface may be depleted, creating anaerobic zones. Under these conditions, incomplete degradation of hydrocarbons can result in the formation of methane gas. Methane is readily biodegradable aerobically, contributes to oxygen depletion, and may affect the soil vapor profile of other hydrocarbons. Methane production and transport are not specifically addressed in this document. However, if the methane concentrations (as part of the overall hydrocarbon concentration) are within the range of simulated source concentrations and pressure-driven advection of methane does not occur, then the model results presented in this report should be generally applicable. It should be noted that methane may be the dominant vapor component (present at 1 to 20 percent by volume) at some petroleum sites. These sites may include ebullition of methane gas resulting in increased soil gas pressures with advective flow of soil gas. The effect of methane gas generation on petroleum vapor intrusion was not simulated in this study, but has been explored by Jourabchi et al. (2012).

### **2.3.6 Model Input Parameters**

Model input parameters, including soil physical properties, are listed in Table 2. These parameters are reasonably representative of typical conditions and were held constant during the modeling runs. A homogeneous sandy soil was used for the base cases and simulations were run for various lengths of time to determine if quasi-steady state conditions had been achieved or to verify the time frame of transport time before oxygen is depleted. Additional scenarios were run for a sandy soil overlain by a one meter thick layer of silty clay. All simulations were run with a single fraction of recalcitrant organic carbon in the soil. Results under transient conditions (including the time to reach a quasi-steady state condition) are affected by the fraction of recalcitrant organic carbon due to its effect on transport of certain VOCs. However, the presence or absence of an oxygen shadow in the sub slab would not be affected by the  $f_{oc}$  present in the soil because the  $f_{oc}$  doesn't itself exert an oxygen demand.

## **2.4 Sensitivity Testing**

To evaluate the sensitivity of the model to an initial condition where hydrocarbons are released into a subsurface setting that contains less than atmospheric levels of oxygen, simulations were performed with initial oxygen in soil gas at 10.5 percent by volume instead of 21 percent by

volume. This value is in the range of background vadose zone soil oxygen content, which has been reported in various sources as 5 to 18 percent<sup>3</sup> and 15 to 21 percent<sup>4</sup> by volume.

**Table 2. Model Input Parameters**

<p><b>Building/foundation parameters</b>  Length*: 10 m to 632 m  Width*: 10 m to 632 m  Depth in soil:</p> <ul style="list-style-type: none"> <li>• 2.0 m (basement type)</li> <li>• 0.2 m (slab-on-grade type)</li> </ul> <p>Foundation thickness: 0.15m  Enclosed space volume: (width x length x 2.44) m<sup>3</sup>  Indoor air mixing height: 2.44 m  Air exchange rate: 0.5 h<sup>-1</sup>  Crack width: 0.001 m  Crack location: Perimeter  Building depressurization: 5 Pa</p> <p><b>Soil Properties</b>  Sandy soil:  Soil bulk density: 1,660 kg/m<sup>3</sup>  Moisture-filled porosity: 0.054 m<sup>3</sup> water/m<sup>3</sup> soil  Total soil porosity: 0.375 m<sup>3</sup> voids/m<sup>3</sup> soil  Soil gas permeability: 1E-11 m<sup>2</sup>  Benzene effective diffusion coefficient: 5.12E-3 m<sup>2</sup>/h  Oxygen effective diffusion coefficient: 1.16E-2 m<sup>2</sup>/h</p> <p>Silty clay:  Soil bulk density: 1,380 kg/m<sup>3</sup>  Moisture-filled porosity: 0.216 m<sup>3</sup> water/m<sup>3</sup> soil  Total soil porosity: 0.481 m<sup>3</sup> voids/m<sup>3</sup> soil  Soil gas permeability: 1.5E-13 m<sup>2</sup>  Benzene effective diffusion coefficient: 1.65E-3 m<sup>2</sup>/h  Oxygen effective diffusion coefficient: 3.74E-3 m<sup>2</sup>/h</p> <p>F<sub>oc</sub> = 0.001</p>	<p><b>Hydrocarbon vapor source properties</b>  Location: base of vadose zone  Source size: entire domain footprint</p> <p><b>Hydrocarbon properties</b>  Overall effective diffusion coefficient for transport in the porous media: 5.12E-3 m<sup>2</sup>/h  Overall effective diffusion coefficient for transport in the crack: 3.17E-2 m<sup>2</sup>/h  Atmospheric concentration: 0.0 mg/L  Henry's Law constant (H<sub>i</sub>): 0.228 m<sup>3</sup> water/m<sup>3</sup> vapor  Sorption coefficient of hydrocarbon to organic carbon (K<sub>oc,i</sub>): 61.7 kg/kg organic carbon  First order biodegradation rate = 0.79 h<sup>-1</sup></p> <p><b>Oxygen properties</b>  Overall effective diffusion coefficient for transport in porous media: 1.16E-2 m<sup>2</sup>/h  Overall effective diffusion coefficient for transport in the crack: 7.2E-2 m<sup>2</sup>/h  Henry's Law constant (H<sub>i</sub>): 31.6 m<sup>3</sup> water/m<sup>3</sup> vapor  Sorption coefficient of oxygen to organic carbon (K<sub>oc,i</sub>): negligible, assumed 0 kg/kg oc  Ratio of oxygen to hydrocarbon consumed:</p> <ul style="list-style-type: none"> <li>• 3 kg-oxygen/kg-hydrocarbon</li> </ul> <p>Threshold concentration: 1% vol/vol  Atmospheric concentration: 21% vol/vol</p> <p><b>Others</b>  Dynamic viscosity of air: 0.0648 Kg/m/h</p> <p>NOTE: model input parameters in this table are provided in metric units only because the model requires metric units.</p>
---	--

<sup>3</sup> <http://www.colorado.edu/engineering/civil/CVEN4474/resources/Biovent.pdf>

<sup>4</sup> <http://www.afcee.af.mil/resources/technologytransfer/programsandinitiatives/bioventing/sitescreening/index.asp>

---

To evaluate the time frame before oxygen was depleted and to evaluate the oxygen conditions when a quasi-steady transport condition was achieved, simulations were conducted with increasing transport times.

Simulation results (see Tables B-1 through B-5 in Appendix B) indicate that the probability of an oxygen shadow developing increases with:

- Building size
- Source vapor strength
- Decreasing vadose zone thickness between source and building slab (source distance from slab)
- Transport time for oxygen consumption under transient conditions

## **2.5 Potentially Confounding Factors**

The following factors can increase the concentration of oxygen in the subsurface, but were not included in the model simulations. As a result the model may overestimate the formation of an oxygen shadow:

- Wind-induced advection. Wind impinging on buildings and topography can induce pressure differences in soil gas, thus inducing a sub-horizontal flow of soil gas under buildings, which may increase the rate of oxygen replenishment under a building, and reduce the potential for shadow formation (Parker, 2003; Lundegard et al., 2008).
- Barometric-induced advection. Diurnal and longer-period barometric pressure fluctuations can induce the flow of soil gas into and out of shallow soils. This barometrically-induced advection may affect the rate of oxygen replenishment under a building.
- Bi-directional soil gas exchange through foundation openings. Cracks and openings in building foundations have been shown to have bidirectional flow, depending on the differential pressure between the building and the adjacent soil gas (McHugh et al., 2006). During periods of positive differential pressure, oxygen may enter the subsurface through the foundation, thus increasing the rate of oxygen replenishment and decreasing the tendency for shadow formation.
- Aerated foundation course. Many slab-on-grade buildings are constructed with a layer of gravel or other coarse-grained material beneath the slab. This coarse-grained layer may provide a conduit or plenum for enhanced advection of air under the building, which may provide a protective blanket of oxygen-rich soil gas under the building (Lundegard et al., 2008).
- Source depletion. The model assumes that the source does not deplete and has a constant concentration beneath the full extent of the foundation.
- Permeable concrete. The model assumes the foundation concrete is impermeable and doesn't account for the potential transport of oxygen through the foundation. In

---

reality, concrete may allow slow diffusion of oxygen from the building into the subsurface even in the absence of discrete openings or cracks.

- Moisture limitation under the building. As discussed in section 2.2, the model used does not simulate water infiltration and associated effects the building may have on limiting the infiltration of soil moisture beneath the slab. If moisture in the soils immediately below the building fell to below 25 percent of field capacity, then biodegradation in that area could be limited and the model may over predict the consumption of oxygen. However, in cases where the petroleum hydrocarbon source is associated with the groundwater table, a layer with both adequate moisture and oxygen is likely to exist within the soil column.

In contrast, the following factors can decrease the concentration of oxygen in the subsurface, but were not included in the model simulations. As a result the model may underestimate the formation of an oxygen shadow.

- High natural oxygen consumption from unusually highly organic content soils (i.e., peat)
- The presence of high concentrations of other gases providing a carbon substrate for microbial metabolism, such as methane, whether derived from the anaerobic biodegradation of ethanol-blended gasoline or anaerobic degradation of conventional petroleum fuels
- Shallow soil layers with high moisture content that restricts oxygen flux to the subsurface (Lundegard et al., 2008)
- Regional coverage of a high percentage of the ground surface by impervious or lower permeability materials, as may occur in major city centers. Information sources on land cover derived from satellite or aerial photography data can be accessed from the United States Geological Survey (USGS) Land Cover Institute <http://landcover.usgs.gov/index.php>
- A vadose zone composed solely or principally of bedrock with little or no overlying soils

Therefore, while these simulations may give an indication of the potential for oxygen shadow formation under worst case conditions dominated by diffusive flow, they should not be regarded as accurate predictions of actual performance at all field sites.

---

### **3. Results and Discussion**

#### **3.1 Summary of Tabulated Results**

The results from model simulations are summarized in Tables B-1 through B-5 in Appendix B. Tables B-1 through B-4 present results for slab-on-grade buildings. Tables B-1 through B-3 present results for a vadose zone consisting of a homogeneous sandy soil with vapor source depths of the following:

- 5 ft (1.6 m) – Table B-1
- 15 ft (4.6 m) – Table B-2
- 30 ft (9 m) – Table B-3

In Tables B-1 through B-3, the results for square building footprints are presented first, followed by results for rectangular buildings. Within each group of building shape, the results are presented in order of increasing source vapor concentration and foundation size.

Table B-4 presents the results for simulations run with a 3.3 ft (1 m) silty clay layer overlying sand. Table B-5 presents results for buildings with a basement.

In the summary table, an oxygen shadow is qualitatively defined to occur when the predicted oxygen content in soil gas beneath the slab is less than or equal to 1 percent by volume (Abreu and Johnson, 2006; Abreu et al., 2009a,b; Ward et al., 1997; Patterson and Davis, 2009). The minimum oxygen concentration immediately below the slab and 3.3 ft (1 m) below the slab is also tabulated.

#### **3.2 Graphical Conventions Used in Figures**

The 3-D model calculates the chemical vapor concentration in the subsurface, the mass flow rates into the building(s), and the indoor air concentration due to vapor intrusion. To facilitate the discussion and the presentation of results, the model output has been normalized using the source concentration (i.e., the predicted concentration is divided by the maximum vapor concentration in the subsurface). The normalized concentrations shown in the figures can be multiplied by the source concentration (or initial oxygen concentration, as appropriate) to convert into absolute concentrations. The hydrocarbon concentration contour lines in most of the figures show these normalized soil vapor concentrations, which are always dimensionless and range from 0 to 1, with 1 being equal to the source concentration.

Since the simulations presented in this document assume a homogeneous soil system with an infinite source footprint, there is symmetry in the soil gas concentration profile with relation to the centerline of the building (Abreu and Johnson, 2006). Figures 3, 4, and 5 illustrate graphical conventions used in analogous figures showing model results. Figure 3 shows a plot of the PHC vapor profile beneath the full width of a large building as well as the corresponding half building plot; notice that the contours are essentially identical. Figure 4 shows the corresponding oxygen profiles beneath the full width of a large building and the corresponding half building. As with Figure 3, the contours are essentially identical.

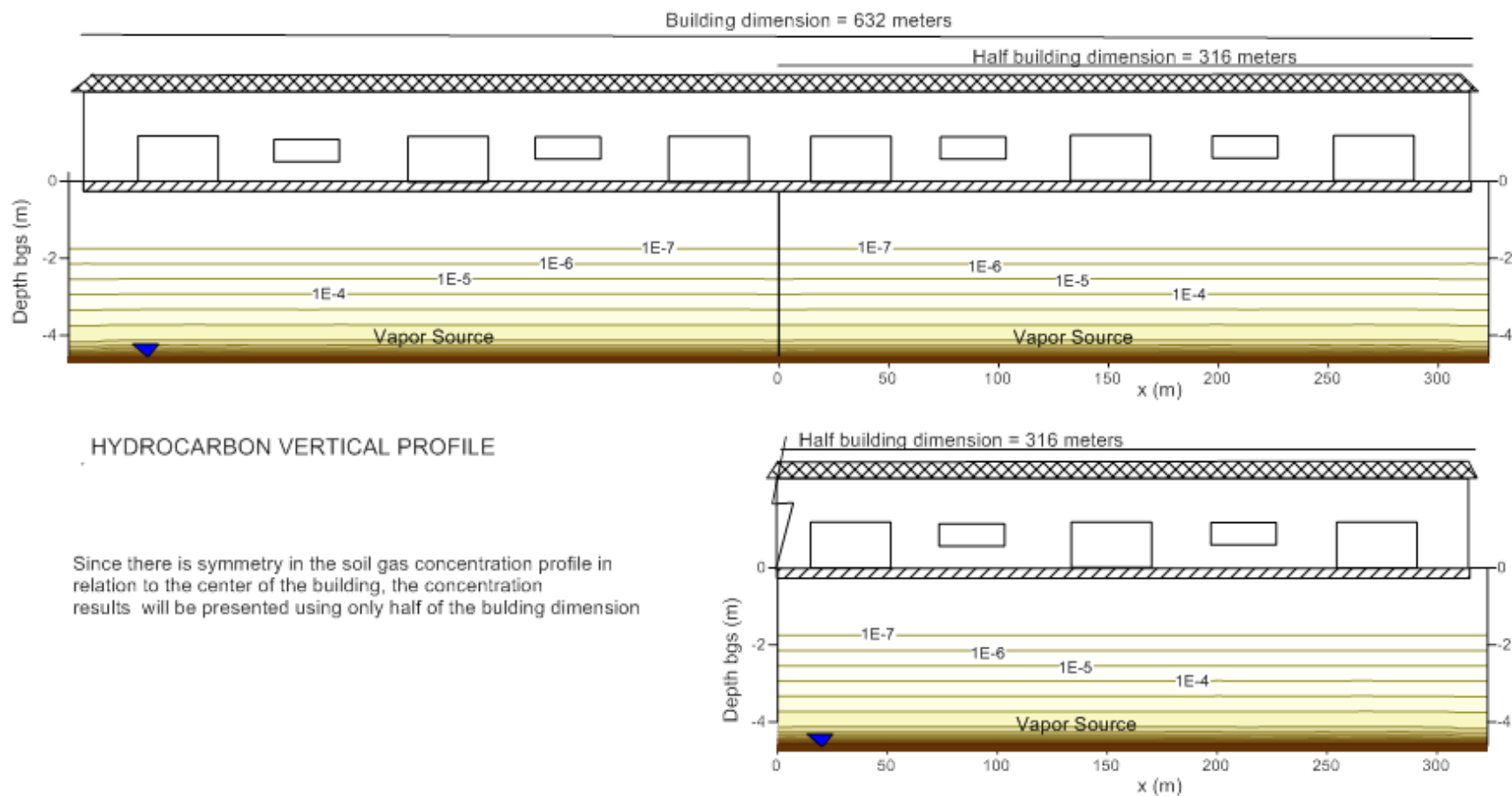
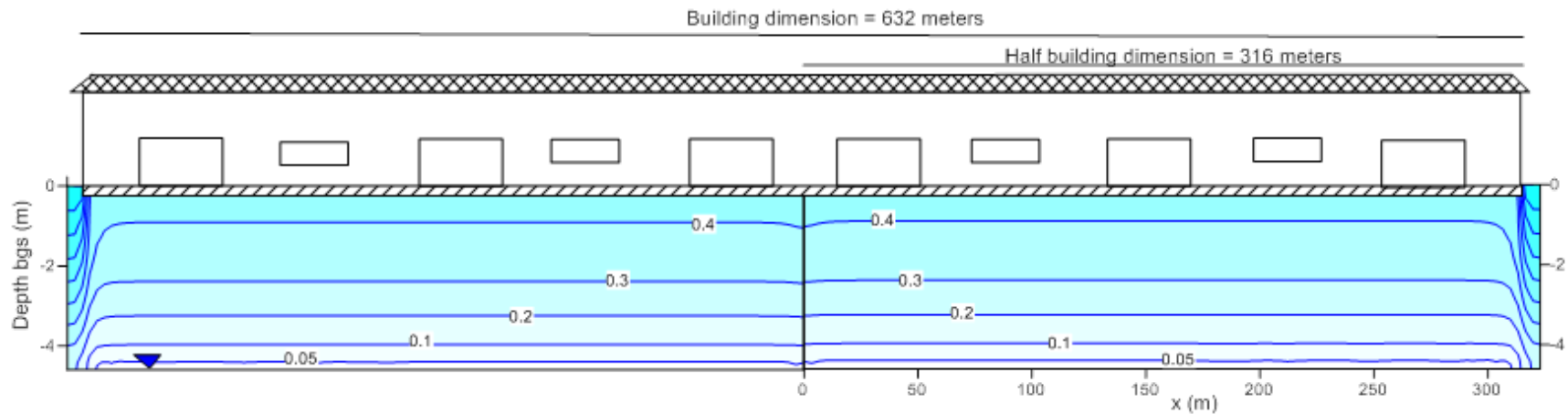


**Figure 3. Contours of simulated petroleum hydrocarbon vapors in the subsurface beneath a building. Results for PHC source vapor concentration of  $10,000,000 \mu\text{g}/\text{m}^3$  at depth of 15 ft (4.6 m) and building size of 2,073 ft x 2,073 ft (632 m x 632 m). Initial oxygen concentration of 21 percent by volume and transport time of 20 days.**





#### OXYGEN VERTICAL PROFILE

Since there is symmetry in the soil gas concentration profile in relation to the center of the building, the concentration results will be presented using only half of the building dimension

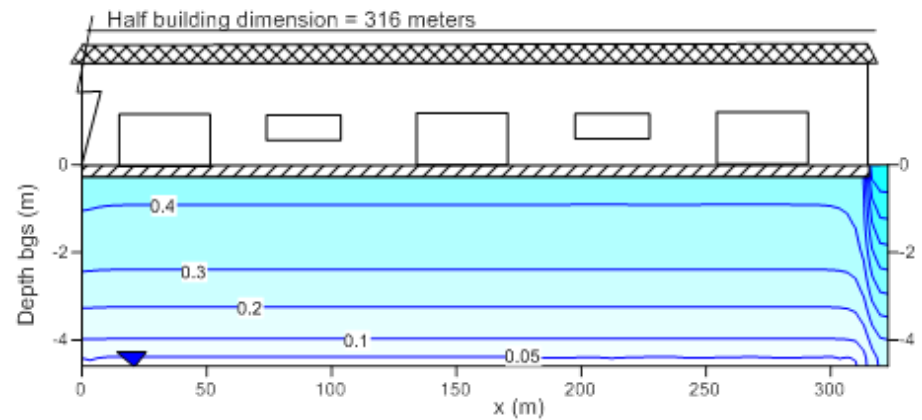


**Figure 4.** Contours of simulated oxygen concentrations in the subsurface beneath a building. Results for PHC source vapor concentration of  $10,000,000 \mu\text{g}/\text{m}^3$  at depth of 15 ft (4.6 m) and building size of 2,073 ft x 2,073 ft (632 m x 632 m). Initial oxygen concentration of 21 percent by volume and transport time of 20 days.

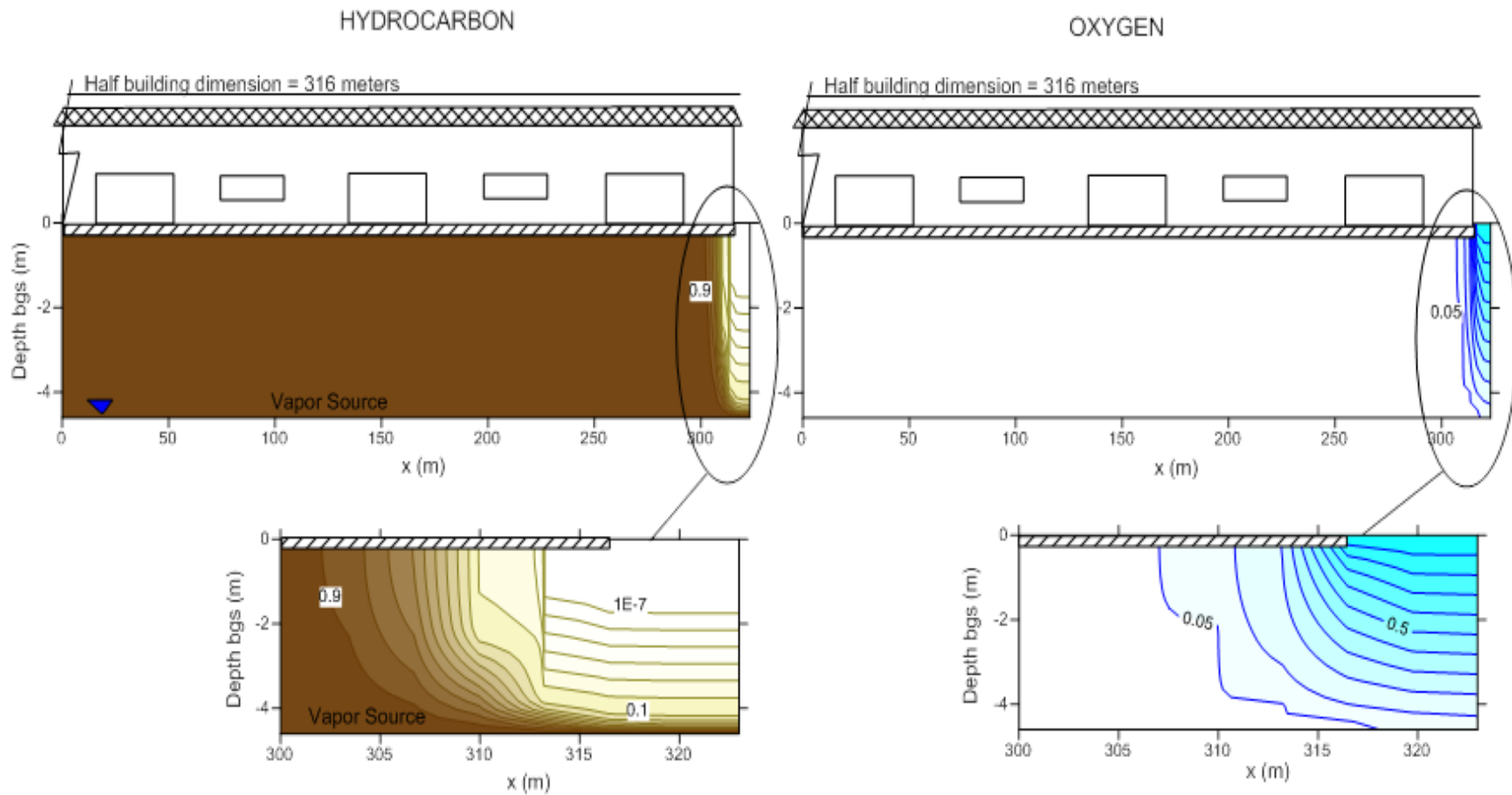


**Figure 5. Expanded view of portion of the 7 meter model domain outside the building footprint. Results for source vapor concentration of 10,000,000  $\mu\text{g}/\text{m}^3$  at depth of 15 ft (4.6 m) and building size of 2,073 ft x 2,073 ft (632 m x 632 m). Initial oxygen concentration of 21 percent by volume and transport time of 1 year.**

---

For both Figure 3 and Figure 4, the results are for a source with vapor concentration of  $10,000,000 \mu\text{g}/\text{m}^3$  and simulated transport time of 20 days; there is no oxygen shadow nor hydrocarbon vapor build up below the slab. Figure 5 shows profiles for both PHC vapor and oxygen concentrations beneath a building for the same scenario simulated in Figures 3 and 4 but for a longer transport time (1 year), and the results show the oxygen shadow and hydrocarbon vapor build up below the slab. Note that in all of the model scenarios, the model domain extends horizontally beyond the building footprint for a distance of 23 ft (7 m). However, due to the scale of the plot, the contours beyond the building are compressed and difficult to distinguish. However, close up plots of this region (see the ovals drawn on Figure 5) reveal that at the far boundary, the concentration isopleths are horizontal. This indicates that even under high source vapor concentration conditions, the 7 m distance to the far boundary in the modeled domain provides a sufficient surface area to allow for oxygen infiltration. Thus, the results are not sensitive to further increases in the size of the modeled domain, and extension of the domain (which would increase computational burden) is unnecessary.

### 3.3 Results for a Homogeneous Sandy Soil and Square Buildings

Results for simulations for homogeneous sandy soil are presented in Appendix B, Tables B-1 through B-3. As shown in Figure 6 and Figure 7, no oxygen shadow develops beneath the largest building simulated (2,073 ft x 2,073 ft [632 m x 632 m]) with relatively low source vapor concentrations ( $10,000 \mu\text{g}/\text{m}^3$  and  $100,000 \mu\text{g}/\text{m}^3$ ) even when the source is shallow (5 ft [1.6 m]) and the transport time is long (50 years). Therefore, it can be inferred that no oxygen shadow would develop if the source vapor concentration is at or below  $100,000 \mu\text{g}/\text{m}^3$  and with a thicker vadose zone. However, as shown in Figure 8, when the source vapor concentration is increased to  $1,000,000 \mu\text{g}/\text{m}^3$  and the source depth is only 5 ft (1.6 m), an oxygen shadow develops after a period of 6 to 9 years under the same large building. Figure 9 shows that when the source depth is increased to 15 ft (4.6 m) and the source concentration is held at  $1,000,000 \mu\text{g}/\text{m}^3$ , no oxygen shadow forms even after 20 years. If the initial oxygen concentration in the soil gas is reduced to 10.5 percent by volume then an oxygen shadow does develop (Figure 10). Extending the transport time to 50 years has a similar effect. As shown in Figure 11, with the highest source vapor concentration modeled ( $10,000,000 \mu\text{g}/\text{m}^3$ ), an oxygen shadow develops in less than one year after release for the 15 ft (4.6m) vadose zone thickness combined with the largest modeled building size 2,073 ft x 2,073 ft (632 m x 632 m). Therefore, it can be inferred that an oxygen shadow has a greater potential to occur when the vadose zone is thinner than 15 ft (4.6 m) and the source vapor concentrations are in the range of  $10,000,000 \mu\text{g}/\text{m}^3$ . In fact, under these conditions, an oxygen shadow develops in less than one year beneath a building with dimensions of 98 ft x 98 ft (30 m x 30 m); no oxygen shadow developed for buildings with a smaller footprint (Figure 12 and Table B-2).

For a small building with dimensions of 33 ft x 33 ft (10 m x 10 m) underlain by the highest source vapor concentration modeled ( $10,000,000 \mu\text{g}/\text{m}^3$ ) and a shallow 5 ft (1.6 m) vadose zone, an oxygen shadow forms rapidly (Table B-1).

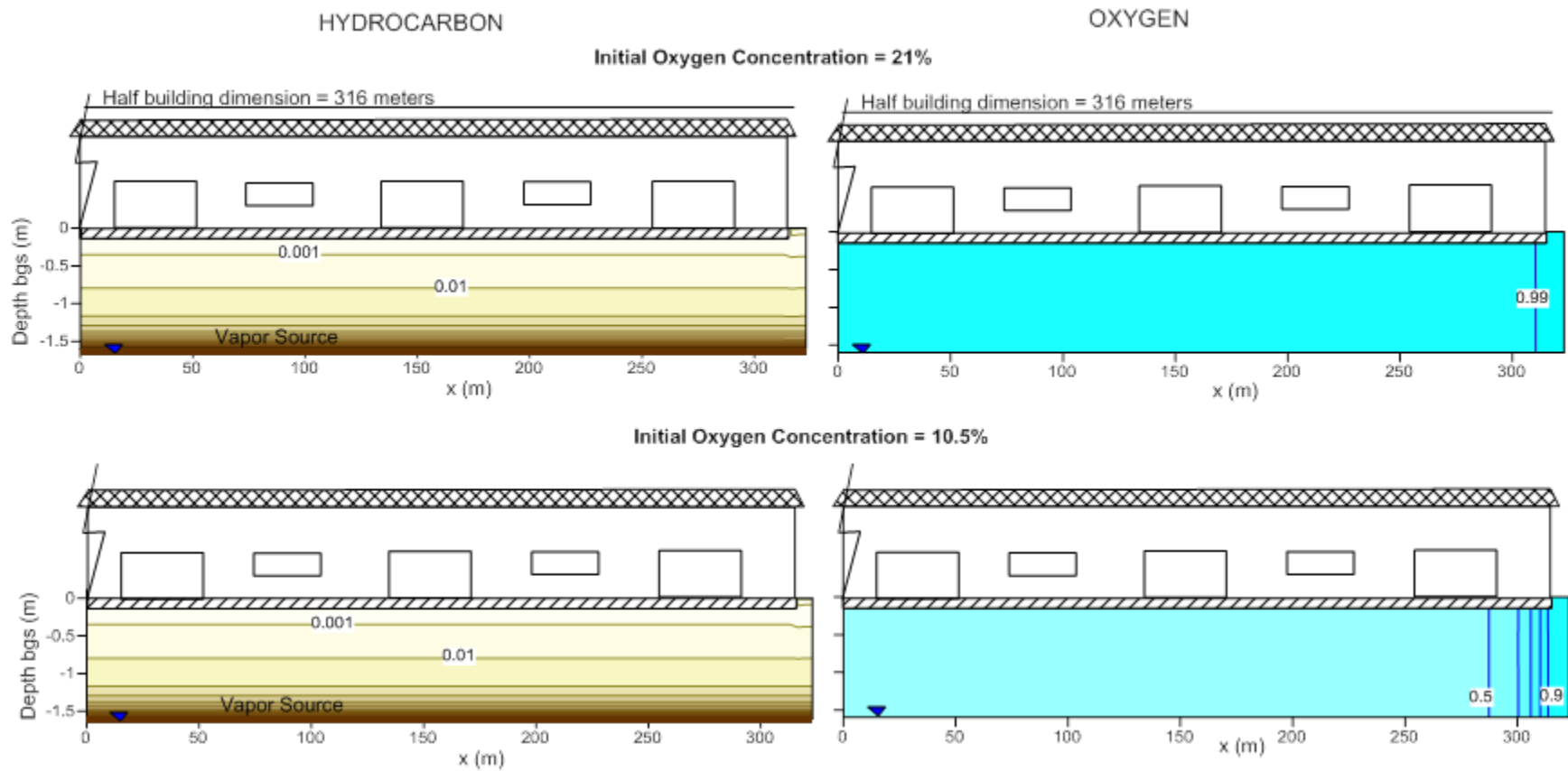
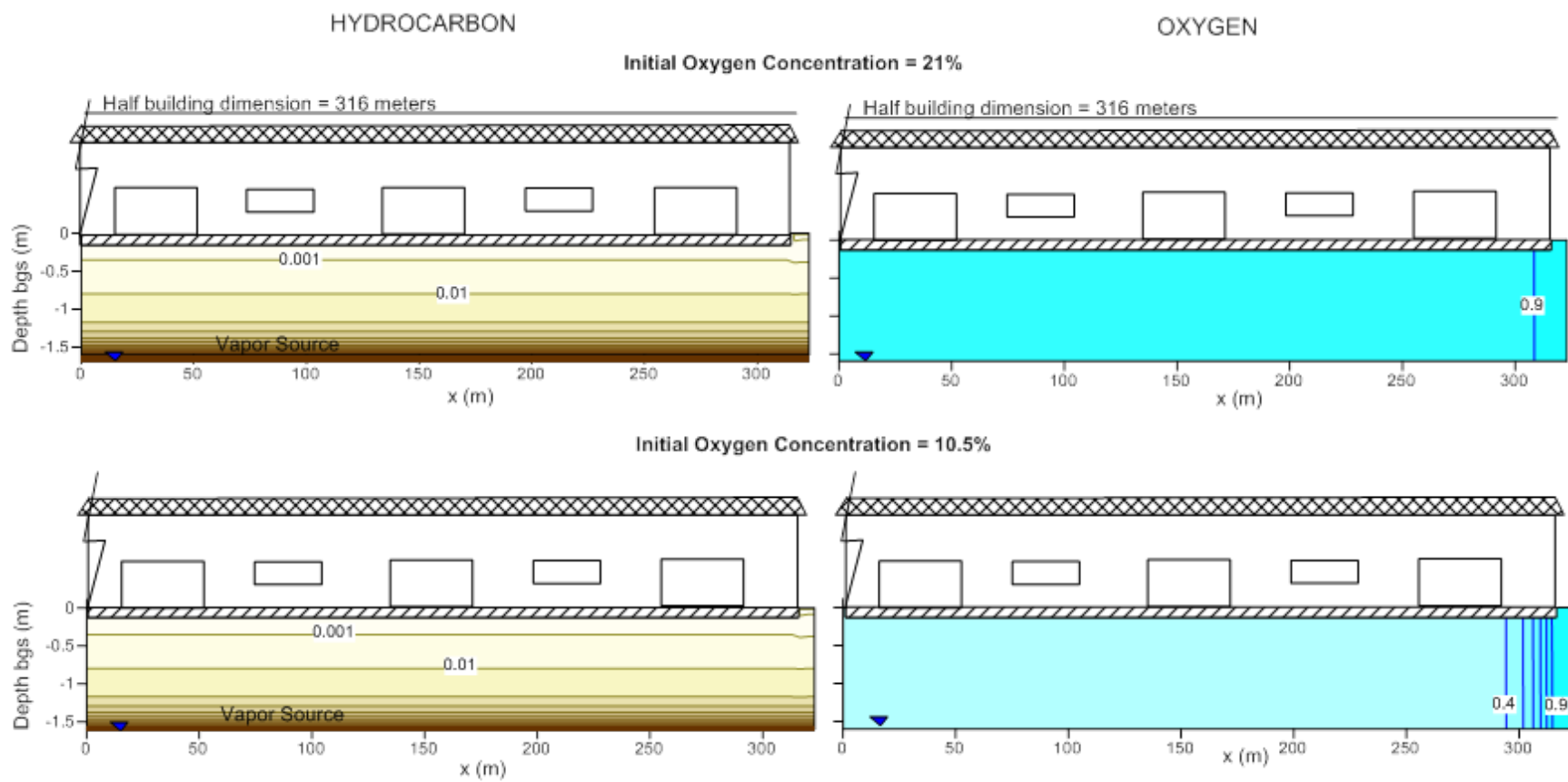
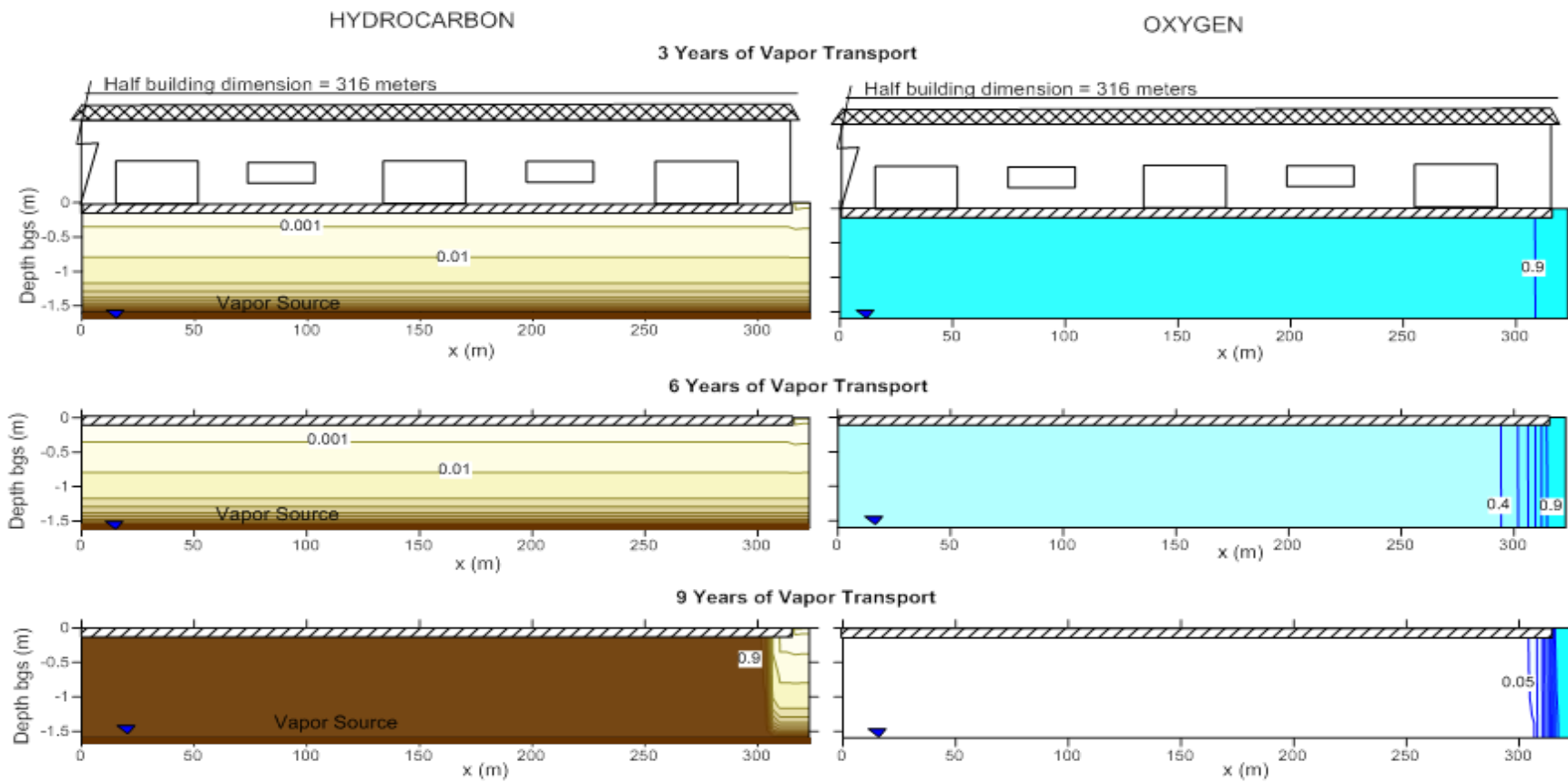


Figure 6. Concentration results for source vapor concentration of  $10,000 \mu\text{g}/\text{m}^3$  at depth of 5 ft (1.6 m) and building size of 2,073 ft x 2,073 ft (632 m x 632 m). Initial oxygen concentration of 21 and 10.5 percent by volume and transport time of 20 years.



**Figure 7.** Concentration results for source vapor concentration of  $100,000 \mu\text{g}/\text{m}^3$  at depth of 5 ft (1.6 m) and building size of 2,073 ft x 2,073 ft (632 m x 632 m) over sandy soil. Initial oxygen concentration of 21 and 10.5 percent by volume and transport time of 20 years.



**Figure 8.** Concentration results for source vapor concentration of  $1,000,000 \mu\text{g}/\text{m}^3$  at depth of 5 ft (1.6 m) and building size of 2,073 ft x 2,073 ft (632 m x 632 m). Initial oxygen concentration of 21 percent by volume and transport times of 3, 6 and 9 years.

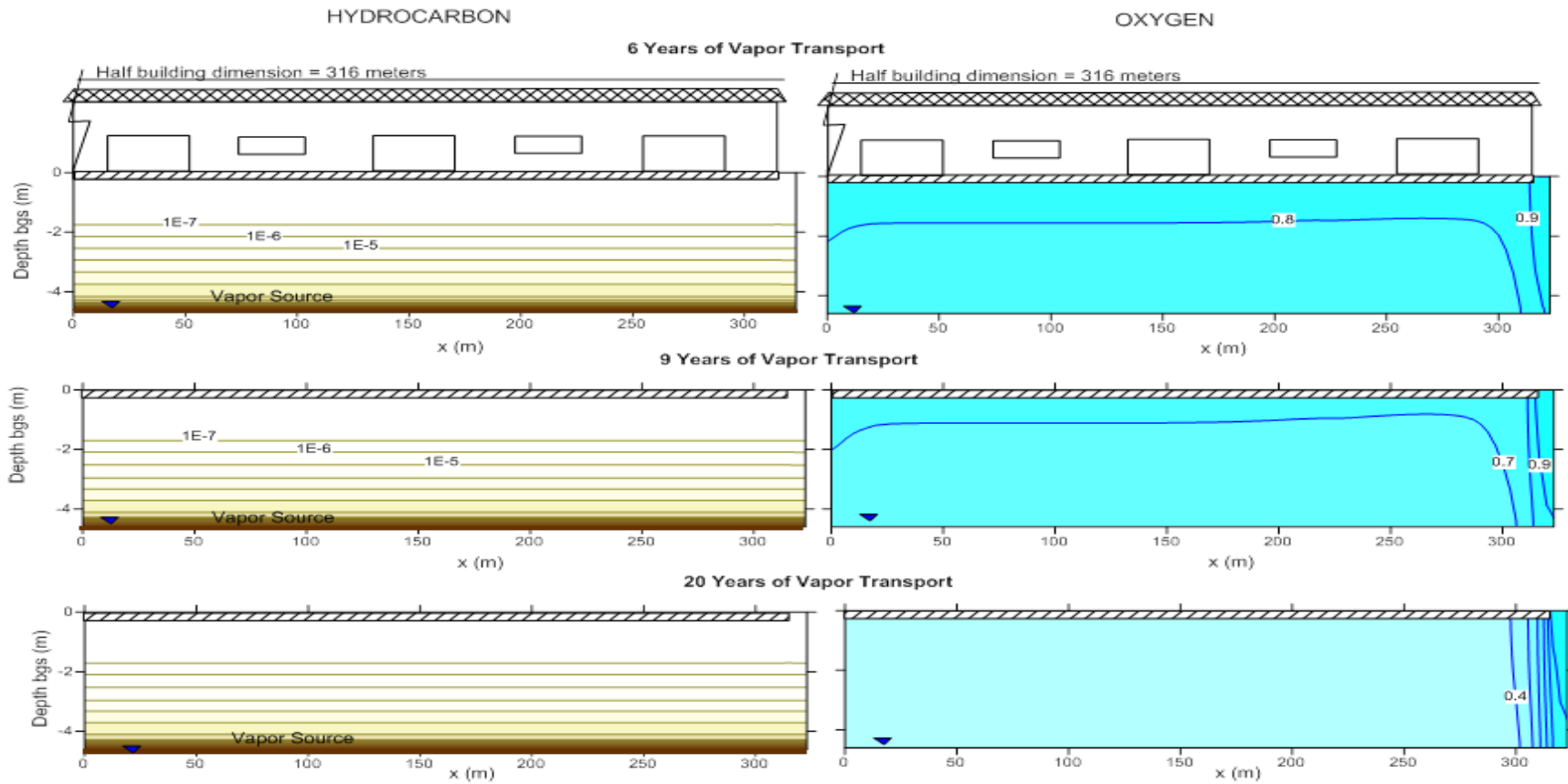


Figure 9. Concentration results for source vapor concentration of  $1,000,000 \mu\text{g}/\text{m}^3$  at depth of 15 ft (4.6 m) and building size of 2,073 ft x 2,073 ft (632 m x 632 m) Initial oxygen concentration of 21 percent by volume and transport times of 6, 9 and 20 years.

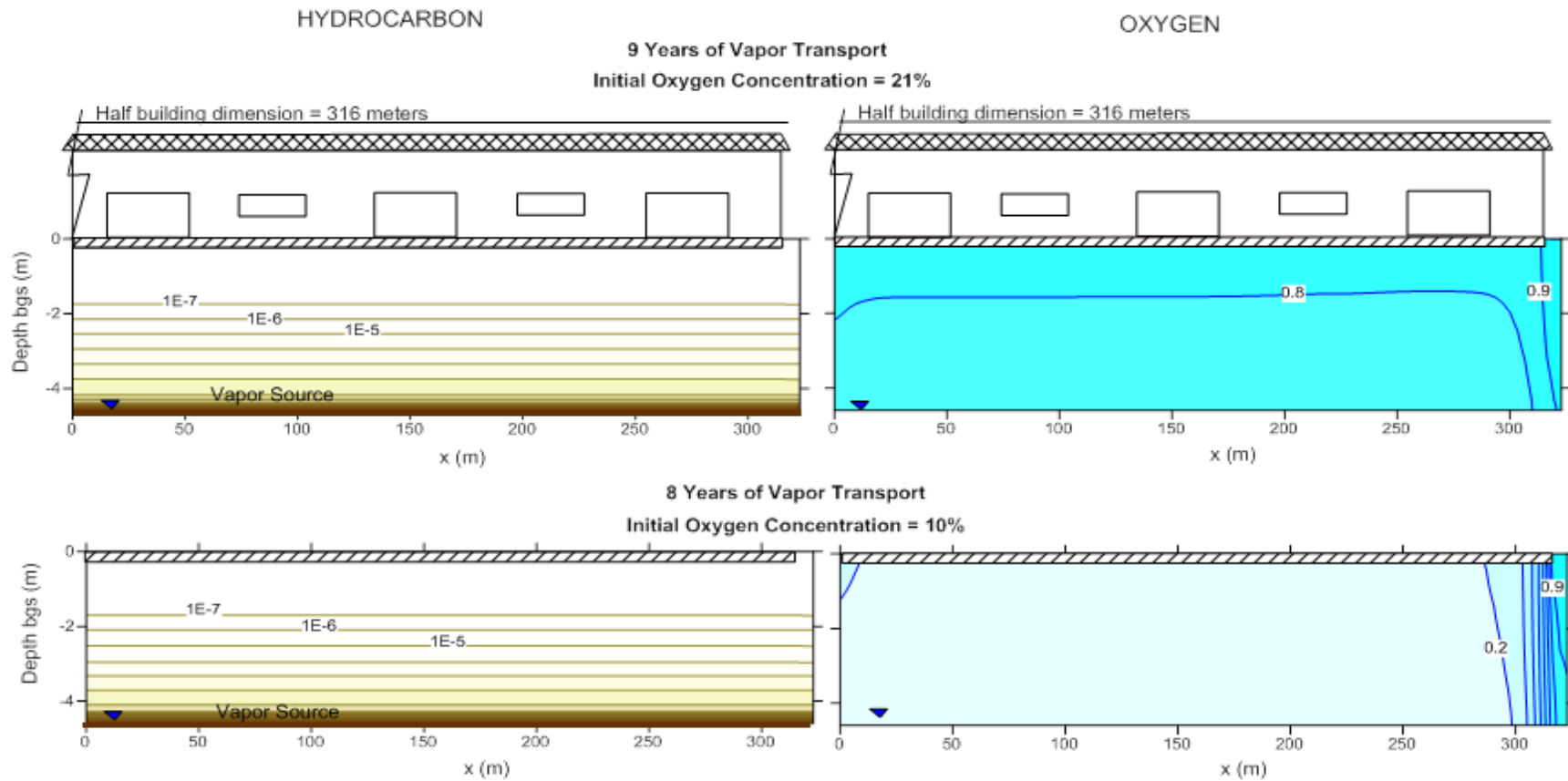


Figure 10. Concentration results for source vapor concentration of  $1,000,000 \mu\text{g}/\text{m}^3$  at depth of 15 ft (4.6 m) and building size of 2,073 ft x 2,073 ft (632 m x 632 m) for an initial concentration of oxygen at 21% and 10% and transport times of 8 and 9 years.



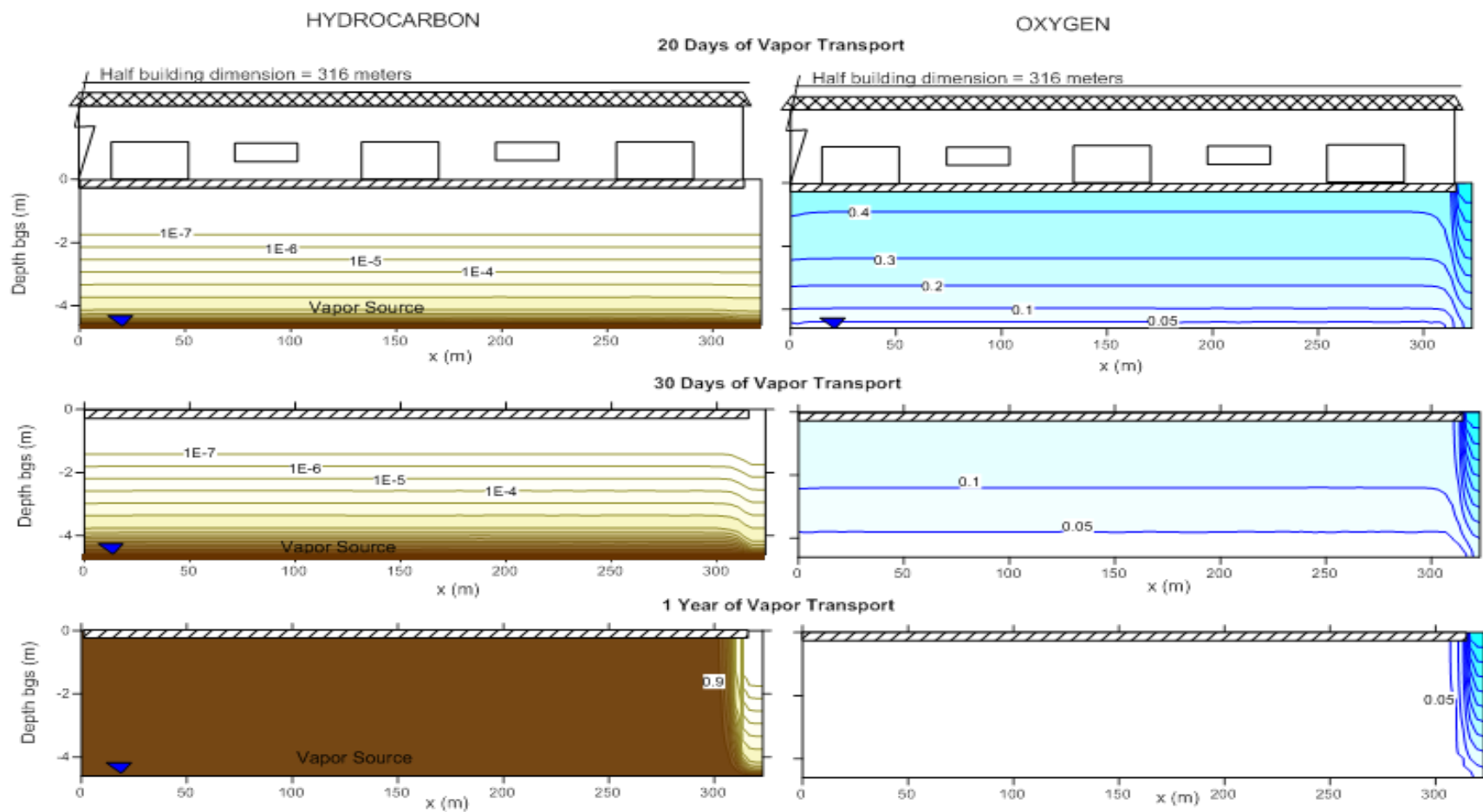


Figure 11. Concentration results for source vapor concentration of  $10,000,000 \mu\text{g}/\text{m}^3$  at depth of 15 ft (4.6 m) and building size of 2,073 ft x 2,073 ft (632 m x 632 m) Initial oxygen concentration of 21 percent by volume. Three transport time: 20 days, 30 days and 1 year (steady state condition within one year of transport).

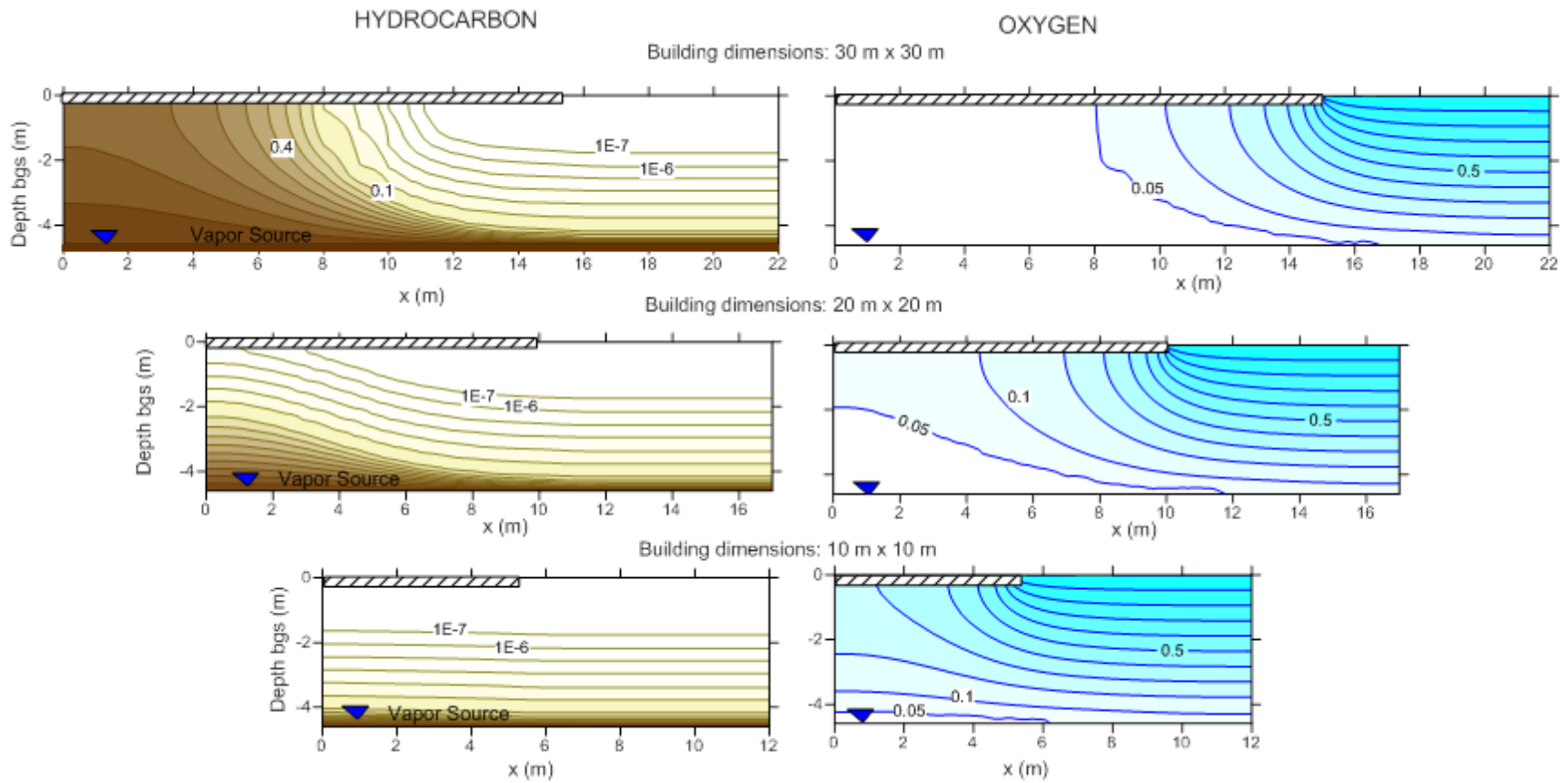


Figure 12. Concentration results for source vapor concentration of  $10,000,000 \mu\text{g}/\text{m}^3$  at depth of 15 ft (4.6 m) and three building sizes: 98 ft x 98 ft, 66 ft x 66 ft and 33 ft x 33 ft (30 m x 30 m, 20 m x 20 m, and 10 m x 10 m). Initial oxygen concentration of 21 percent by volume and steady state condition within one year of transport.

---

For the highest source vapor concentration modeled ( $10,000,000 \mu\text{g}/\text{m}^3$ ) and a relatively large vadose zone thickness (30 ft: 9 m) only a limited number of simulations were run. The results show that oxygen is substantially depleted and rapidly comes to a steady state condition. However, the oxygen does not quite reach the operational definition of an oxygen shadow for buildings between 98 ft x 98 ft (30 m x 30 m) and 131 ft x 131 ft (40 m x 40 m) (Figure 13 and Table B-3). An oxygen shadow does form beneath a building of 197 ft x 197 ft (60 m x 60 m).

Results for higher source vapor concentrations and small 33 ft x 33 ft (10 m x 10 m) buildings are shown in EPA (2012, Section 5), and Abreu and Johnson (2006). U.S EPA 2012 summarizes for sources at 26 ft (8 m) bgs in a uniform sand:

*“The concentration profiles for the basement scenario . . . show that for source vapor concentrations of  $100,000,000$  and  $200,000,000 \mu\text{g}/\text{m}^3$  (representative of weathered gasoline NAPL sources), oxygen is consumed before it can penetrate beneath the foundation. Thus, no biodegradation is occurring beneath the foundation in the region below the 0.05 oxygen contour line, because of limited oxygen availability and supply. In this region, the vapor transport is not attenuated by biodegradation. As a result, the hydrocarbon concentration is higher below the foundation compared with similar depths away from the building with sufficient oxygen for biodegradation. For a source vapor concentration of  $20,000,000 \mu\text{g}/\text{m}^3$ , oxygen penetrates beneath the entire foundation. The vapor transport is attenuated by biodegradation throughout much of the subsurface, and the vertical profile of the hydrocarbon concentration is similar beneath the building and away from the building. The concentration profiles for the slab-on-grade scenario show an increased oxygen supply beneath the foundation relative to the basement scenario, and the vapor transport is therefore attenuated by biodegradation beneath the entire building footprint, even for the highest source concentrations simulated. The differences in the aerobic zone (oxygen) distribution beneath the slab-on-grade foundation compared with the basement foundation are due to the combination of a smaller distance for oxygen transport from the atmosphere and an increased distance for hydrocarbon transport from the source to locations immediately beneath the slab. The concentration profiles in the subsurface away from the foundation are identical for both scenarios (basement and slab-on-grade).”* (U.S. EPA, 2012). Note: units converted from the original for compatibility with this report).

### **3.4 Results for a Homogeneous Sandy Soil and Rectangular Buildings**

Several rectangular building simulations were performed for shallow vapor sources at 5 ft (1.6 m). Three simulations were performed for a very thin building footprint 33 ft x 2,073 ft (10 m x 632 m) with a source vapor concentration of  $1,000,000 \mu\text{g}/\text{m}^3$ . These simulations came to quasi-steady state with a stable concentration of oxygen at 15.6 percent by volume. This oxygen concentration is substantially higher in comparison to the scenario with a very large square building (2,073 ft x 2,073 ft: 632 m x 632 m) that resulted in development of an oxygen shadow beneath the building. In contrast, this result is similar to the base case where the building was square with dimensions of 33 ft x 33 ft (10 m x 10 m) that resulted in only a slight decrease (from 21 percent to 17.8 percent) in the oxygen concentration beneath the building (Table B-1). This result is consistent with the expectation for rectangular buildings discussed in Section 2.3.1.

---

Additional simulations with rectangular buildings were also performed at the depth of 15 ft (4.6 m) with a long, thin 33 ft x 295 ft (10 m x 90 m) building. With the highest source vapor concentration of 10,000,000  $\mu\text{g}/\text{m}^3$  quasi-equilibrium was reached with a stable oxygen concentration of 4 percent by volume. These results are comparable to those (6.1 percent oxygen) for a square building of 33 ft x 33 ft (10 m x 10 m). Even when the extreme bounding case of a 33 ft x 2,073 ft (10 m x 632 m) building shape was simulated, quasi-equilibrium was reached with a stable oxygen concentration of 4.1 percent by volume (Figure 14 and Table B-2). These results provide further support for the expectation for rectangular building discussed in Section 2.3.1.

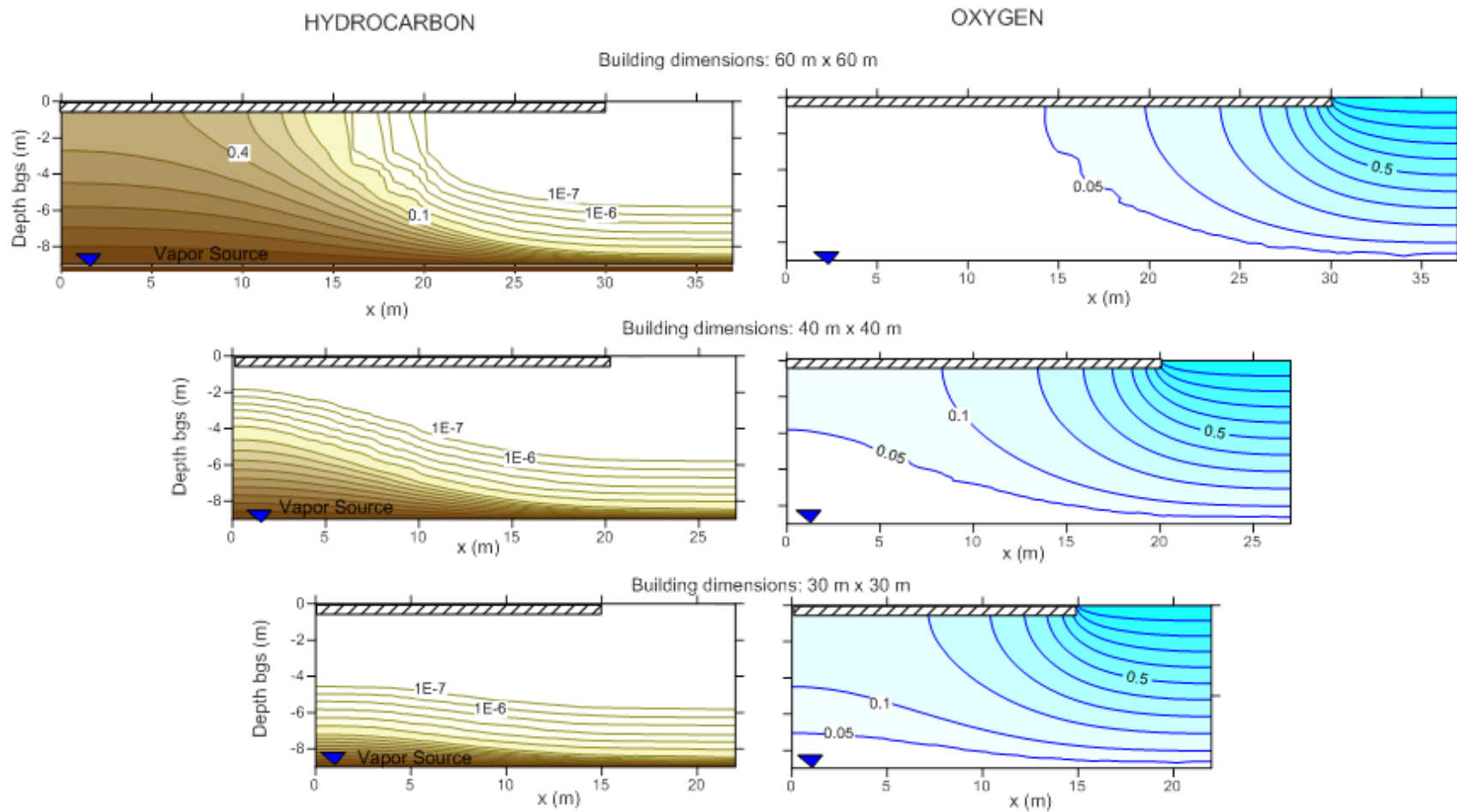


Figure 13. Concentration results for source vapor concentration of  $10,000,000 \mu\text{g}/\text{m}^3$  at depth of 30 ft (9 m) and three building sizes: 197 ft x 197 ft, 131 ft x 131 ft and 98 ft x 98 ft (60 m x 60 m, 40 m x 40 m, and 30 m x 30 m). Initial oxygen concentration of 21 percent by volume and steady state condition within one year of transport.

---

Thus, the depletion of oxygen beneath a rectangular building is controlled primarily by the dimension of the short side of the floor plan (i.e., the shortest distance from the slab center to the edge of the building) (see Figure 14). The minimum oxygen concentration in the rectangular buildings will be slightly lower than would be expected for a square building with the same length as the smaller side of the rectangular building.

### **3.5 Results for a Homogeneous Sandy Soil with an Overlying Silty Clay Layer at Ground Surface**

Approximately thirty simulations were conducted with a 3 ft (1 m) thick silty clay layer acting as a capping layer on top of an underlying homogeneous sandy soil (Table B-4). For simulations with the source at a depth of 5 ft (1.6 m), the silty clay layer comprises the majority of the simulated vadose zone. Thus, the resulting oxygen transport is substantially lower than the base case where sandy soil comprised the entire thickness of the vadose zone. For example, beneath the largest building 2,073 ft x 2,073 ft (632 m x 632 m) and with the source vapor concentration of 100,000  $\mu\text{g}/\text{m}^3$ , a minimum oxygen concentration of 1 percent by volume is reached beneath the slab in 20 years, although depletion of oxygen began within only 9 years (Table B-4). This stands in contrast to the corresponding scenario for a sandy soil, which still had an oxygen concentration of 17.9 percent by volume beneath the slab after 20 years of simulated transport (Table B-1).

Similarly, for a medium sized square building (98 ft: 30 m on a side) with a source vapor concentration of 1,000,000  $\mu\text{g}/\text{m}^3$  at a depth of 5 ft (1.6 m) and beneath the shallow silty clay layer, an oxygen shadow forms within 9 years (Table B-4). This stands in contrast to the corresponding all-sand condition, where the oxygen was 12.3 percent by volume after 9 years had elapsed (Table B-1).

At the vadose zone thickness of 15 ft (4.6 m) with the 3.2 ft (1 m) silty clay layer at the surface and a source vapor concentration of 1,000,000  $\mu\text{g}/\text{m}^3$  an oxygen shadow forms in 9 years (Table B-4). Without the silty clay layer, the corresponding simulations do not reach oxygen concentration of 1 percent by volume until between 20 and 50 years had elapsed.

With the largest vadose zone thickness modeled (30 ft: 9 meters) and a source vapor concentration of 10,000,000  $\mu\text{g}/\text{m}^3$  the overlying clay layer still reduces the oxygen flux to the subsurface. For example, with the 98 ft x 98 ft (30 m x 30 m) building footprint the oxygen concentration beneath the building is reduced from 2.9 to 1.9 percent by volume. With a 131 ft x 131 ft (40 m x 40 m) building footprint, an oxygen shadow forms after 6 years (Tables B-3 and B-4).

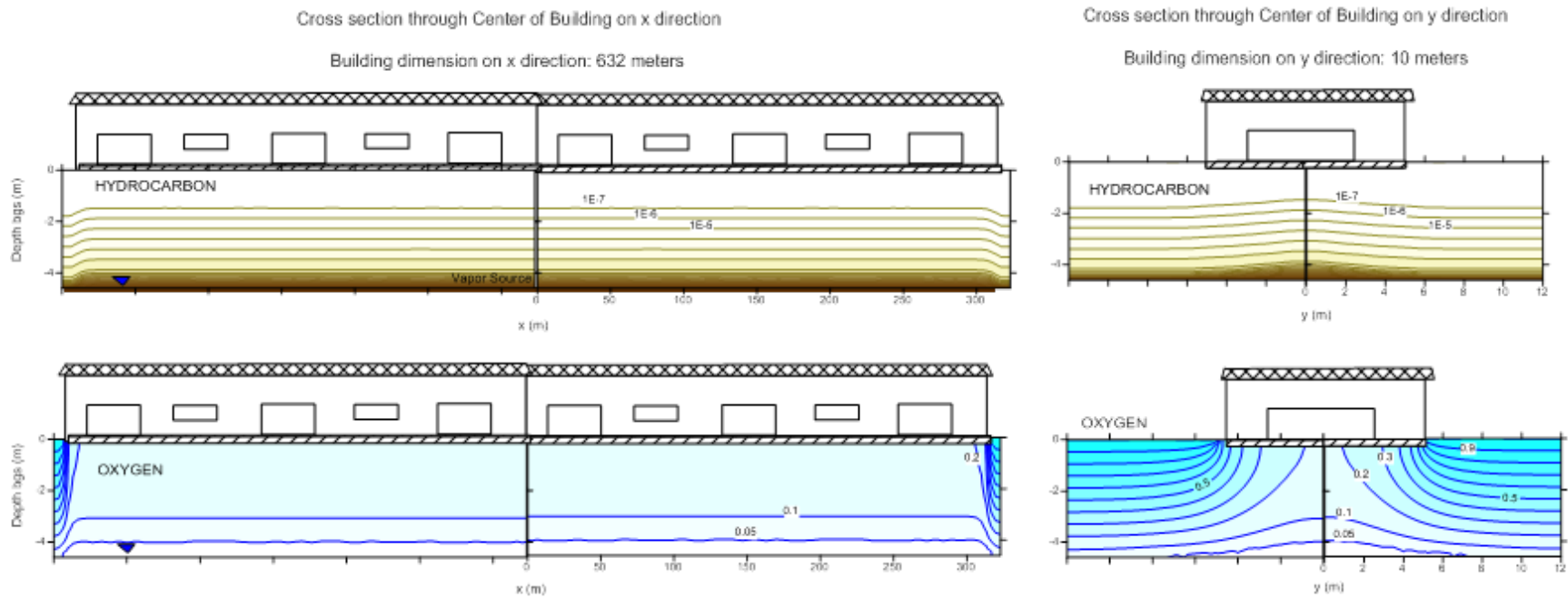


**Figure 14. Concentration results for a building with rectangular shape 2,073 ft x 33 ft (632 m x 10 m), source vapor concentration of 10,000,000  $\mu\text{g}/\text{m}^3$  at 15 ft (4.6 m), initial oxygen concentration of 21 percent by volume and steady state condition. Results viewed in two perpendicular cross sections by center of building.**

---

### 3.6 Results for Buildings with a Basement

Five simulations were performed for a very large building 2,073 ft x 2,073 ft (632 m x 632 m) with a 6.6 ft (2 m) deep basement (Table B-5 and Figure 15) and the source located 5 ft (1.6 m) below the basement slab. The results are essentially the same as those for the corresponding slab-on-grade scenario with a source located 5 ft (1.6 m) below the slab (Table B-1). The results presented in Table B-1 for slab-on-grade and source at 5 ft (1.6 m) bgs are applicable to basement scenarios with a basement depth of 6.6 ft (2 m) and source depth of 12 ft (3.6 m) bgs. Although there may be some slight differences (due to the atmospheric ground surface boundary being further away in the basement scenario) the overall results are essentially the same.

Abreu and Johnson (2006), Abreu et al. (2009a,b) and EPA (2012) presented a significant number of biodegradation scenarios that compared soil vapor and oxygen profiles for buildings with a basement versus slab-on-grade. The results in all four of these investigations are consistent and indicate that the primary controlling factor is the separation distance between the vapor source and the overlying foundation slab, and not the particular construction of the foundation (i.e., slab versus basement).

Figure 16 shows the results of a basement scenario and the corresponding slab-on-grade scenario for a very large building (2,073 ft x 2,073 ft: 632 m by 632 m) with a full basement.



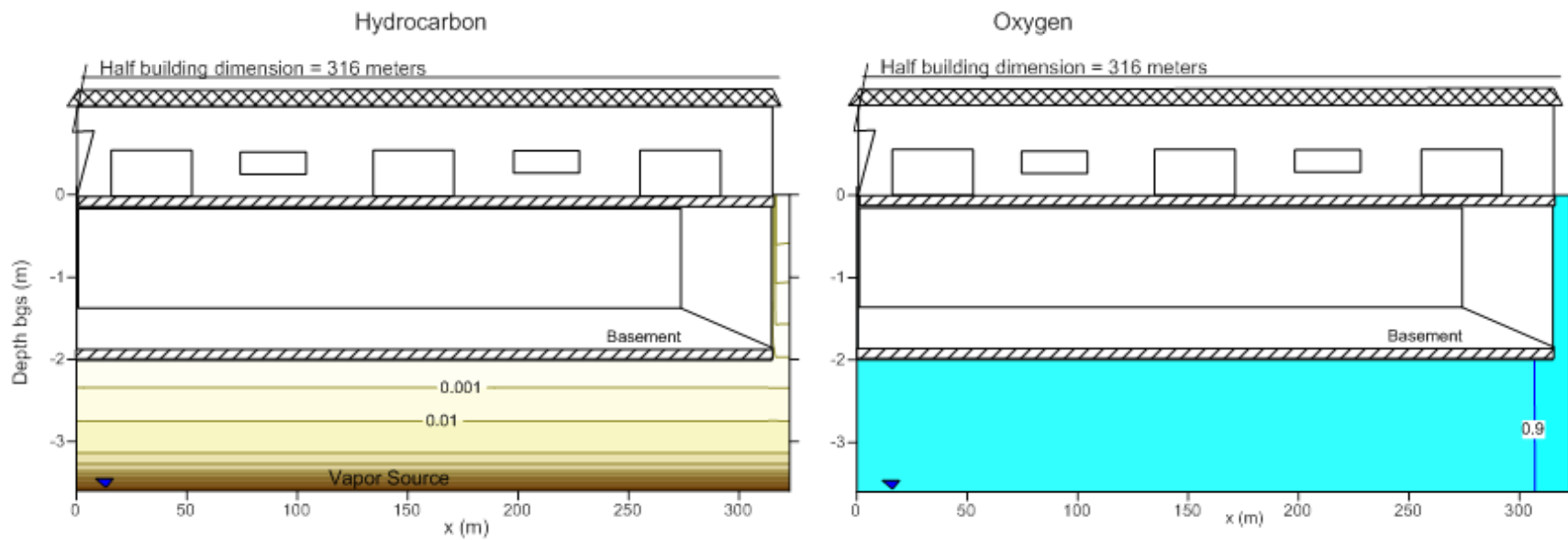


Figure 15. Concentration results for building 2,073 ft x 2,073 ft (632 m x 632 m), with full 6.6 ft (2 m) deep basement, source vapor concentration of  $100,000 \mu\text{g}/\text{m}^3$  at 5 ft (1.6 m) below basement slab, transport time 9 years and initial oxygen concentration of 21 percent by volume.

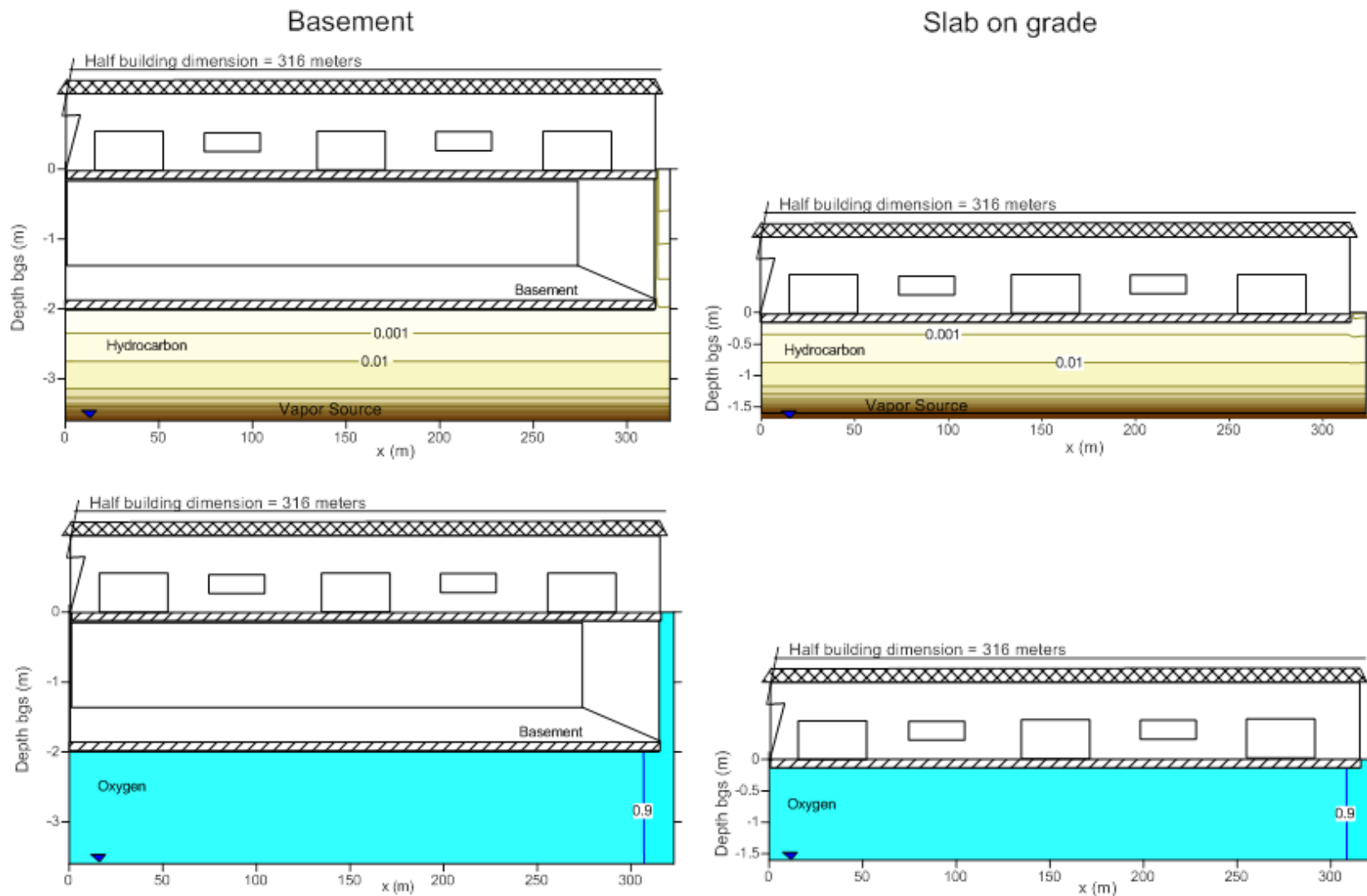


Figure 16. Concentration results for building with full 2 m deep basement vs. building slab-on-grade, for building area 2,073 ft x 2,073 ft (632 m x 632 m), source vapor concentration of 100,000  $\mu\text{g}/\text{m}^3$  at 5 ft (1.6 m) below foundation slab, transport time 9 years and initial oxygen = 21 percent by volume..

---

*[This page intentionally left blank.]*

---

## 4. Conclusions

The results of this study may help practitioners identify situations where they should confirm with field measurements the presence of oxygen necessary to support aerobic biodegradation of petroleum hydrocarbons. Conversely, there are other situations where practitioners can reasonably infer from site conditions the presence of oxygen.

The results of approximately 160 simulations (see Tables B-1 through B-5 in Appendix B) show that the presence or absence of an oxygen shadow is dependent on the following:

- Increasing building area (including surrounding pavement area)
- Increasing source vapor concentration
- Decreasing depth of vapor source beneath the building
- Increasing transport time for oxygen consumption under transient conditions (assuming the source PHC vapor concentrations are stable)

At lower source vapor concentrations (up to  $100,000 \mu\text{g}/\text{m}^3$ ) an oxygen shadow does not develop even beneath very large buildings (tested cases ranged up to 2,073 ft x 2,073 ft: 632 m x 632 m) with shallow 5 ft (1.6 m) vadose zone, after a long simulated transport time (50 years).

At the intermediate vapor concentration modeled in this report ( $1,000,000 \mu\text{g}/\text{m}^3$ ):

- An oxygen shadow did not form beneath a medium size building, 98 ft x 98 ft (30 m x 30 m) with a shallow 5 ft (1.6 m) vadose zone after a simulated transport time of 9 years
- An oxygen shadow did develop under a building with dimensions of 131 ft x 131 ft (40 m x 40 m) with a shallow 5 ft (1.6 m) vadose zone after a simulated transport time of 9 years
- An oxygen shadow did not form beneath the largest building simulated, 2,073 ft x 2,073 ft (632 m x 632 m) with a moderate thickness vadose zone 15 ft (4.6 m) after a simulated transport time of 20 years

At the highest vapor concentration modeled in this report ( $10,000,000 \mu\text{g}/\text{m}^3$ ):

- An oxygen shadow developed within one year beneath a small building 33 ft x 33 ft (10 m x 10 m) with a shallow 5 ft (1.6 m) vadose zone
- An oxygen shadow developed within one year beneath a medium size building 98 ft x 98 ft (30 m x 30 m) with a moderate thickness vadose zone 15 ft (4.6 m)
- An oxygen shadow did not develop under a building with dimensions of 66 ft x 66 ft (20 m x 20 m) with a moderate thickness vadose zone 15 ft (4.6 m) even after a simulated transport time of 20 years

---

At source vapor concentrations of 1,000,000  $\mu\text{g}/\text{m}^3$ , the simulations indicated that a longer transport time is required for the concentrations to reach quasi-steady state, and oxygen concentrations are still above the threshold for a period of time before it is eventually depleted. This may be interpreted as the result of a flux balance. If diffusion is the dominant transport mechanism, then the following two processes are finely balanced:

- Upward diffusion of hydrocarbons
- Downward and lateral diffusion of oxygen

It is very likely that the modeled results would change significantly if additional processes were modeled, such as high permeability layers beneath building slabs, wind speed/direction variability and bi-directional flow through foundation cracks and penetrations throughout the floor plan. However those factors may be more difficult to identify during a site screening process than the inputs in the current modeling (such as foundation dimensions and thickness of the vadose zone).

The depletion of oxygen beneath a rectangular building is controlled primarily by the dimension of the shorter side of the floor plan.

---

## 5. References

- Abreu, L.D.V.; Ettinger, R.A. and McAlary, T. 2009a. Simulated Soil Vapor Intrusion Attenuation Factors Including Biodegradation for Petroleum Hydrocarbons. *Ground Water Monitoring & Remediation*. 29(1):105-117.
- Abreu, L.D.V.; Ettinger, R. A. and McAlary, T. 2009b. *Simulating the Effect of Aerobic Biodegradation on Soil Vapor Intrusion into Buildings: Evaluation of Low Strength Sources Associated with Dissolved Gasoline Plumes*. API Publication 4775, April. American Petroleum Institute, Regulatory and Scientific Affairs Department, Washington, DC.
- Abreu, L.D.V.; Ettinger, R.A. and McAlary, T. 2007. *Application of 3-D Numerical Modeling to Assess Vapor Intrusion Screening Criteria for Petroleum Hydrocarbon Sites*. *Proceeding of the AWMA Specialty Conference, Vapor Intrusion: Learning from the Challenges*. September 26-28. Providence, RI.
- Abreu, L.D.V. and Johnson, P.C. 2006. Simulating the Effect of Aerobic Biodegradation on Soil Vapor Intrusion into Buildings: Influence of Degradation Rate, Source Concentration, and Depth. *Environmental Science and Technology*. 40(7): 2304-2315.
- Abreu, L.D.V. and Johnson, P.C. 2005. Effect of Vapor Source-Building Separation and Building Construction on Soil Vapor Intrusion as Studied with a Three-Dimensional Numerical Model. *Environmental Science and Technology*. 39(12):4550-4561.
- Abreu, L.D.V. 2005. *A Transient Three-dimensional Numerical Model to Simulate Vapor Intrusion into Buildings*. UMI 3166060, Ph.D. Dissertation, Arizona State University, Tempe, AZ.
- Abu-Irshaid and K.J. Renken. 2002. Relationship Between the Permeability Coefficient of Concrete and Low-Pressure Differentials. *2002 International Radon Symposium Proceedings*. [http://www.aarst.org/proceedings/2002/2002\\_01\\_Relationship\\_Between\\_the\\_Permeability\\_Coefficient\\_of\\_Concrete\\_and\\_Low-Pressure\\_Differentials.pdf](http://www.aarst.org/proceedings/2002/2002_01_Relationship_Between_the_Permeability_Coefficient_of_Concrete_and_Low-Pressure_Differentials.pdf) (accessed 2/19/13).
- Boeing. Undated. Future of Flight Aviation Center and Boeing Tour: Background Information. <http://www.boeing.com/commercial/tours/background.html>, <http://www.boeing.com/commercial/tours/gw.html> and [http://www.boeing.com/commercial/tours/images/K64532-14\\_lg.jpg](http://www.boeing.com/commercial/tours/images/K64532-14_lg.jpg)
- Brown, E. R., M.R. Hainin, A. Cooley and G. Hurley. 2004. *Relationship of Air Voids, Lift Thickness and Permeability in Hot Mix Asphalt Pavements*. National Cooperative Highway Research Program (NCHRP) Report 531, Washington DC.
- Ching, F.D.K. and C. Adams. 2001. *Building Construction Illustrated*. 3<sup>rd</sup> Edition, John Wiley and Sons, NY.

- 
- Colorado Asphalt Pavement Association. 2006., *A Guideline for the Design and Construction of Asphalt Parking Lots in Colorado*, January. <http://www.co-asphalt.com/documents/asphaltparkinglotdesignguide1.pdf> (accessed 2/19/13).
- Davis, G.B., B.M. Patterson and M.G. Trefry. 2009. Evidence for Instantaneous Oxygen-Limited Biodegradation of Petroleum Hydrocarbon Vapors in the Subsurface. *Ground Water Monitoring & Remediation*. 29(1):126-137.
- DeVaull, G.E. 2007. Indoor vapor intrusion with oxygen-limited biodegradation for a subsurface gasoline source. *Environmental Science and Technology*. 41(9):3241–3248.
- DeVaull, G. 2011. Biodegradation Rates for Petroleum Hydrocarbons in Aerobic Soils: A Summary of Measured Data. Slides presented at *International Symposium on Bioremediation and Sustainable Environmental Technologies*, June, Reno Nevada.
- Eklund, B. and D. Burrows. 2009. Prediction of Indoor Air Quality from Soil-gas Data at Industrial Buildings. *Groundwater Monitoring & Remediation*. 29(1): 118-125.
- Florida Concrete & Products Association. Undated. *Concrete Parking Lots, Design Construction Procedures and Specifications*. <http://www.fcpa.org/uploads/FCPADesignConstructionSpecifications.pdf> accessed 2/19/13.
- Gogula, A. K., M. Hossain and S.A. Romanoschi. 2004. *A Study of Factors Affecting the Permeability of Superpave Mixes in Kansas*. November. Report K-Tran: SSU-00-2 to Kansas Department of Transportation. <ftp://ftp.mdt.mt.gov/research/LIBRARY/K-TRAN-KSU-00-2.PDF> accessed 2/19/13.
- Johnson, P.C, C.C. Stanley, M.W. Kemblowski, D.L. Byers, and J.D. Colthart. 1990. A Practical Approach to the Design, Operation and Monitoring of In Situ Soil-Venting Systems. *Ground Water Monitoring & Remediation*. 10(2):159-178.
- Jourabchi, P., N. Sihota, I. Hers, K.U. Mayer, G. DeVaull, R. Kolhatkar, and B. Bauman. 2012. *Effects of Ethanol Blended Gasoline Release on Soil Vapor Transport: Preliminary Results of Biogas Generation Experiments and Numerical Modeling*. Paper #22, Air & Waste Management Association Conference on Vapor Intrusion, Denver Colorado, October 3-4.
- King County, Washington. Undated. *Stormwater Glossary of Terms and Abbreviations*, <http://www.kingcounty.gov/environment/waterandland/stormwater/glossary.aspx#> (accessed 2/20/13).
- Kolhatkar, R., E. Hong Luo and T. Peargin. 2013. Empirical Data to Evaluate the Occurrence of Sub-slab O<sub>2</sub> Depletion ‘Shadow’ at Petroleum Hydrocarbon-Impacted Vapor Intrusion Sites. Slides presented at *The Association for Environmental Health and Sciences (AEHS)*
-

---

*Foundation 23rd Annual International Conference on Soil, Water, Energy, and Air*, San Diego, California, March 2013.

- Lahvis, M. A., I. Hers, R.V. Davis, J. Wright, and G.E. DeVaul. 2013. *Vapor Intrusion Screening at Petroleum UST Sites*, Groundwater Monitoring & Remediation doi: 10.1111/gwmr.12005.
- Koomey, J.G. 1990. *Energy Efficiency in New Office Buildings: An Investigation of Market Failures and Corrective Policies*. Doctoral Dissertation. University of California, Berkeley. <http://enduse.lbl.gov/info/JGKdissert.pdf> accessed February 21, 2012.
- Li. H., J.J Jiao and M. Luk. 2004. A Falling-pressure Method for Measuring Air Permeability of Asphalt in Laboratory. *Journal of Hydrology*. 286:69-77.  
<http://hydro.geo.ua.edu/jiao/research/FullPaper/LiJiao9.pdf> last accessed 2/19/13.
- Lundegard, P.D., P.C. Johnson and P. Dahlen. 2008. Oxygen Transport from the Atmosphere to Soil Gas Beneath a Slab-on-grade Foundation Overlying Petroleum-Impacted Soil. *Environmental Science and Technology*. 42(15):5534-5540.
- McHugh, T.E., P.C. de Blanc, and R.J. Pokluda. 2006. Indoor Air as a Source of VOC Contamination in Shallow Soils below Buildings. *Soil & Sediment Contamination*. 15(1):103–122.
- Michigan Concrete Association. Undated. *Concrete Parking Areas*  
<http://www.miconcrete.org/node/31> accessed 2/19/13.
- Nazaroff, W.W. and A.V. Nero. 1988. *Radon and Its Decay Products in Indoor Air*. John Wiley & Sons, New York, Figure 2.2.
- Parker, J.C. 2003. Modeling Volatile Chemical Transport. Biodecay and Emission to Indoor Air. *Ground Water Monitoring & Remediation*. 23(1):107-120.
- Roggemans, S., C.L. Bruce, and P.C. Johnson. 2001. *Vadose Zone Natural Attenuation of Hydrocarbon Vapors: An Empirical Assessment of Soil Gas Vertical Profile Data*. API Technical Bulletin No. 15. American Petroleum Institute: Washington, DC.
- Sanjuan, M.A. and R. Munoz-Martialay. 1995. Influence of Age on Air Permeability of Concrete. *Journal of Materials Science*. 20:5657-5662.
- Shan, H. Undated. *Hydraulic Conductivity Tests for Soils*. Department of Civil Engineering National Chiao Tung University.  
<http://www.cv.nctu.edu.tw/~wwwadm/chinese/teacher/Ppt-pdf/AGTwk6HydraulicCon.pdf> (accessed 2/19/13).
- Simmons, C.S., J.M. Keller, and J.L. Hylden. 2004. *Spills on Flat Inclined Pavements*. Pacific Northwest National Laboratory Report 14577, March 2004,



- 
- [http://www.pnl.gov/main/publications/external/technical\\_reports/PNNL-14577.pdf](http://www.pnl.gov/main/publications/external/technical_reports/PNNL-14577.pdf) last accessed 2/19/13.
- U.S. Army. 1998. *Concrete and Masonry*. Field Manual 5-428, U.S. Army Headquarters, Washington, DC. 18 June.
- U.S. Census. 2007. *New One-Family Housing Units Sold by Square Feet of Floor Area and Geographic Area*. Table. [http://www.census.gov/const/C25Ann/soldsqft\\_2007.pdf](http://www.census.gov/const/C25Ann/soldsqft_2007.pdf). Last accessed February 21, 2012.
- U.S. EPA. 2013. *Evaluation of empirical data and modeling studies to support soil vapor intrusion screening criteria for petroleum hydrocarbon compounds*, EPA 510-R-13-001. Washington, DC: U.S. Environmental Protection Agency, Office of Solid Waste and Emergency Response. [http://www.epa.gov/oust/cat/pvi/PVI\\_Database\\_Report.pdf](http://www.epa.gov/oust/cat/pvi/PVI_Database_Report.pdf) (accessed April 9, 2013).
- U.S. EPA. 2012. *Conceptual Model Scenarios for the Vapor Intrusion Pathway*. EPA 530-R-10-003. U.S. Environmental Protection Agency, Office of Solid Waste and Emergency Response. <http://www.epa.gov/oswer/vaporintrusion/documents/vi-cms-v11final-2-24-2012.pdf> (accessed April 9, 2013).
- Ward, C. H., J.A. Cherry and M.R. Scalf, eds. 1997. *Subsurface Restoration*. CRC Press.
- Wikipedia. 2012. *List of largest buildings in the world*. [http://en.wikipedia.org/wiki/List\\_of\\_largest\\_buildings\\_in\\_the\\_world](http://en.wikipedia.org/wiki/List_of_largest_buildings_in_the_world) accessed February 21, 2012.
- Winegardener, D.L. and S.M. Testa. 2002. *Restoration of Contaminated Aquifers: Petroleum Hydrocarbons and Organic Compounds*. 2<sup>nd</sup> Edition, CRC Press.

## Appendix A. Model Equations

**Table A-1. Equations Solved by the Numerical Code**

Parameter	Equation
Soil gas disturbance pressure field	$\frac{\partial p}{\partial t} - \left( \frac{\bar{P}}{\phi_g \mu_g} \right) \cdot \vec{\nabla} \cdot (K_g \cdot \vec{\nabla} p) = 0$
Soil gas flow field	$\vec{q}_g = \frac{K_g}{\mu_g} (\vec{\nabla} p)$
Chemical transport: advection, diffusion, and aerobic biodegradation	<p> <math display="block">a \cdot \frac{\partial C_{ig}}{\partial t} = -\vec{\nabla} \cdot (C_{ig} \cdot \vec{q}_g) - \vec{\nabla} \cdot \left( \frac{C_{ig}}{H_i} \cdot \vec{q}_w \right) + \vec{\nabla} \cdot (D \cdot \vec{\nabla} C_{ig}) - R_i</math> </p> <p>where</p> $a = \left( \phi_g + \frac{\phi_w}{H_i} + \frac{K_{oc,i} \cdot f_{oc} \cdot \rho_b}{H_i} \right)$ $D = \left[ D_{ig} + \frac{D_{iw}}{H_i} \right], \quad D_{ig} = d_i^a \frac{\phi_g^{10/3}}{\phi_T^2}, \quad D_{iw} = d_i^w \frac{\phi_w^{10/3}}{\phi_T^2}$ <p><math>R_i</math> is zero if the chemical is recalcitrant. If the chemical is biodegradable then the <math>R_i</math> used in this work is a first-order model limited by oxygen concentration:</p> $\begin{cases} R_i = \phi_w \cdot \lambda_i \cdot C_{iw} & \text{if } C_{oxygen} > C_{og}^{\min} \\ R_i = 0 & \text{if } C_{oxygen} \leq C_{og}^{\min} \end{cases}$ <p>The reaction rate for oxygen (<math>R_o</math>) is determined stoichiometrically:</p> $R_o = \sum_{i=1}^m r_{k_o} \cdot R_i$
Indoor air concentration	$C_{ig}^{indoor} = \frac{E_s + V_b \cdot A_{ex} \cdot C_{i,amb}}{V_b \cdot A_{ex} + Q_s}$ <p>where</p> $Q_s = \int_{L_{ck}} Q_{ck} \cdot dL_{ck}$ <p>and</p> $E_s = \int_{L_{ck}} Q_{ck} \cdot \frac{\left[ \exp \left( \frac{Q_{ck}}{w_{ck} \cdot D_{ck}} d_{ck} \right) C_{ig} - C_{ig}^{indoor} \right]}{\left[ \exp \left( \frac{Q_{ck}}{w_{ck} \cdot D_{ck}} d_{ck} \right) - 1 \right]} \cdot dL_{ck}$

---

## Definitions of Symbols Used in Table A-1

$p$ :	disturbance pressure (absolute atmospheric pressure minus absolute soil gas pressure at a point) $[M/L/T^2]$
$t$ :	time $[T]$
$\bar{P}$ :	mean soil gas pressure (approximated by the atmospheric pressure for the problems of interest here) $[M/L/T^2]$
$\phi_g$ :	gas-filled porosity $[L^3_{\text{gas}}/L^3_{\text{soil}}]$
$\mu_g$ :	soil gas dynamic viscosity $[M/L/T]$
$\vec{\nabla}$ :	vector del operator $[L^{-1}]$
$K_g$ :	soil permeability to soil gas flow $[L^2]$
$\vec{q}_g$ :	soil gas discharge vector $[L^3_{\text{gas}}/L^2_{\text{area}}/T]$
$i$ :	chemical-specific subscript
$C_{ig}$ :	gas-phase concentration of chemical $i$ $[M_i/L^3_{\text{gas}}]$
$\vec{q}_w$ :	soil moisture specific discharge vector $[L^3_{\text{fluid}}/L^2_{\text{area}}/T]$
$R_i$ :	net loss rate of chemical $i$ due to reaction $[M_i/L^3_{\text{soil}}/T]$
$\phi_w$ :	moisture-filled porosity $[L^3_{\text{water}}/L^3_{\text{soil}}]$
$\rho_b$ :	soil bulk density $[M_{\text{soil}}/L^3_{\text{soil}}]$
$f_{oc}$ :	mass fraction of organic carbon in the soil $[M_{oc}/M_{\text{soil}}]$
$K_{oc,i}$ :	sorption coefficient of chemical $i$ to organic carbon $[(M_i/M_{oc})/(M_i/L^3_{\text{water}})]$
$H_i$ :	Henry's law constant for chemical $i$ $[(M_i/L^3_{\text{gas}})/(M_i/L^3_{\text{water}})]$
$D_{ig}$ :	effective porous media diffusion coefficients for chemical $i$ in soil gas $[L^2/T]$
$D_{iw}$ :	effective porous media diffusion coefficients for chemical $i$ in soil moisture $[L^2/T]$
$d_i^a$ :	molecular diffusion coefficient of chemical $i$ in air $[L^2/T]$
$d_i^w$ :	molecular diffusion coefficient of chemical $i$ in water $[L^2/T]$
$\phi_T$ :	total soil porosity $(= \phi_g + \phi_w)$ $[L^3_{\text{pores}}/L^3_{\text{soil}}]$
$\lambda_i$ :	first-order reaction rate $[1/T]$
$C_{oxygen}$ :	oxygen soil gas concentration $[M/L^3\text{-vapor}]$
$rk_o$ :	ratio of oxygen to hydrocarbon consumed $[M_o/M_i]$
$m$ :	total number of aerobically degrading chemicals
$E_s$ :	emission rate of chemical $i$ to enclosed space $[M/T]$
$A_{ex}$ :	enclosed space air exchange rate $[1/T]$
$V_b$ :	enclosed space volume $[L^3]$ where indoor air is assumed fully mixed
$C_{i,amb}$ :	concentration of chemical $i$ in ambient air $[M/L^3]$
$Q_s$ :	soil gas flow rate to the enclosed space $[L^3/T]$
$C_{og}^{\text{min}}$ :	threshold oxygen concentration for aerobic biodegradation to occur.

**Table A-2. Boundary Conditions**

Boundaries	Boundary Condition(s)
All vertical plane-of-symmetry, all lateral boundaries, solid foundation sections, and the lower model domain boundary	$\vec{\nabla} p \cdot \vec{n} = 0$ $\vec{\nabla} C_{ig} \cdot \vec{n} = 0 \text{ (except at the vapor source boundary)}$
Vapor source boundary	$C_{ig} = C_{i,g}^{\text{source}}$
Soil-atmosphere interface	$p^{atm}(t) = 0 \text{ for steady atmospheric pressure, otherwise}$ $p^{atm}(t) = A_1 \cdot \sin(\varphi_1 \cdot t + \theta_1) + A_2 \cdot \sin(\varphi_2 \cdot t + \theta_2)$ $C_{ig} = 0$ $C_{\text{oxygen}} = C_{\text{og}}^{\text{atm}} \quad (0.28 \text{ mg/cm}^3)$
Disturbance pressure within the building	$p^{indoor}(t) = p^{atm}(t) + \Delta p_B(t)$
Foundation crack–soil interface.	$Q_{ck} = \left( -\frac{w_{ck}^3}{12\mu_g \cdot d_{ck}} \right) [p - p^{indoor}] = w_{ck} \left( \frac{K_g}{\mu_g} \right) \frac{\partial p}{\partial z}$ $Q_{ck} \cdot \frac{\left[ \exp\left( \frac{Q_{ck}}{w_{ck} \cdot D_{ck}} d_{ck} \right) \right] C_{ig} - C_{ig}^{indoor}}{\left[ \exp\left( \frac{Q_{ck}}{w_{ck} \cdot D_{ck}} d_{ck} \right) - 1 \right]} =$ $= w_{ck} \cdot \left[ C_{ig} \left( \frac{K_g}{\mu_g} \right) \left( \frac{\partial p}{\partial z} \right) - D \left( \frac{\partial C_{ig}}{\partial z} \right) \right]$

---

## Definitions of Symbols Used in Table A-2

- $\vec{n}$ : unit vector normal to the surface of interest
- $p^{atm}(t)$ : disturbance pressure at the soil-atmosphere interface [M/L/T<sup>2</sup>]
- $p^{indoor}(t)$ : disturbance pressure within the building [M/L/T<sup>2</sup>]
- $\Delta p_B(t)$ : pressure difference between the indoor air and the atmospheric air (or gauge pressure)
- $A$ : user-defined amplitudes [M/L/T<sup>2</sup>]
- $\varphi$ : user-defined frequencies [radians/T]
- $\theta$ : user-defined phases [radians]
- $Q_{ck}$ : soil gas flow rate per unit length of crack [(L<sup>3</sup><sub>gas</sub>/T)/L]
- $w_{ck}$ : crack width [L]
- $d_{ck}$ : foundation thickness [L]
- $C_{og}^{atm}$ : oxygen atmospheric concentration [M/L<sup>3</sup>-vapor]
- $D_{ck}$ : effective diffusion coefficient for transport in the crack [L<sup>2</sup>/T].

## Revision of the Indoor Air Mixing Equation Assumption

The indoor air concentration equation presented in Table A-1 was derived by assuming an instantaneous steady-state condition on the enclosed space mass balance. This assumption did not hold true for high frequency barometric pressure fluctuations; therefore, a revised indoor air mixing equation was derived to properly account for an accumulation term in simulations with transient pressure fluctuations. The revised equation is as follows:

$$C_{ig,m}^{indoor} = \frac{[C_{ig,m-1}^{indoor} \cdot V_b + (E_s + V_b \cdot A_{ex} \cdot C_{i,amb}) \cdot (t_m - t_{m-1})]}{[V_b + (V_b \cdot A_{ex} + Q_s) \cdot (t_m - t_{m-1})]}$$

Where  $m$  is the time step index and all other variables are as defined for Table A-1.

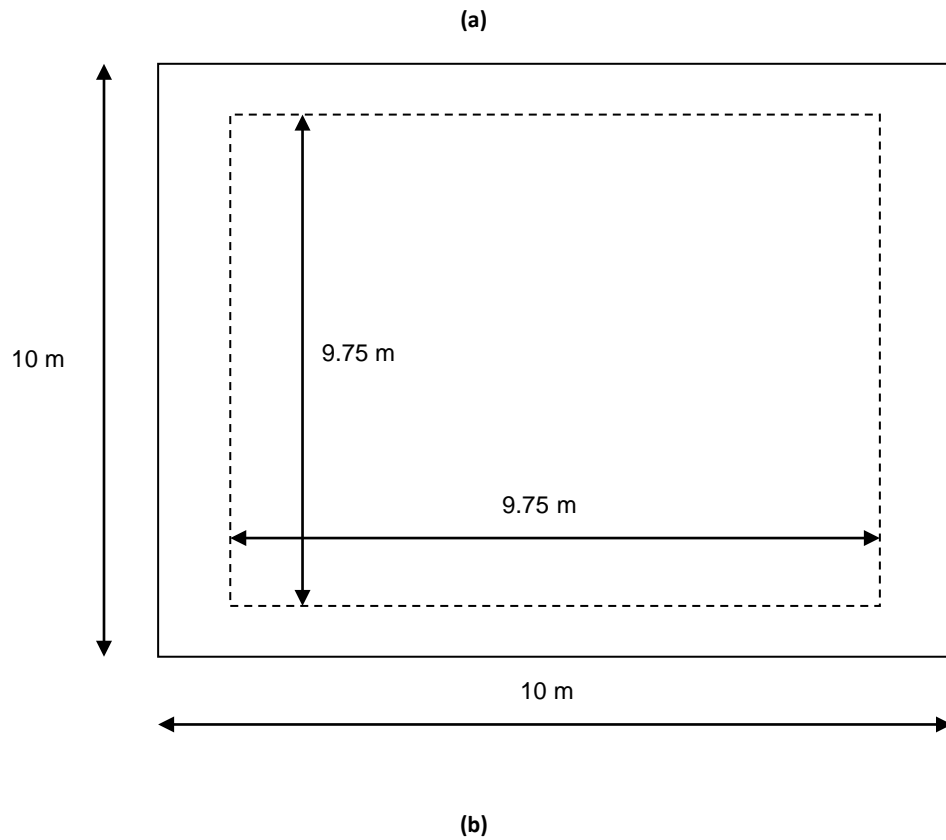


**Figure A-1. Plan view of the foundation crack distribution (dashed lines) used in the simulations for perimeter cracks illustrated for the 10m x 10m case.**

Note that as the building dimensions increase the length of the perimeter cracks also increase and they retain the same distance of 0.25 m from the exterior walls.

---

*[This page intentionally left blank.]*

---

## **Appendix B. Tabulated Simulation Results**



**Table B-1. Matrix Summarizing Simulations Run with Source at 5 ft (1.6 m)**

Full Domain Scale (International Units)								
Geology: Homogeneous Sand								
Source Vapor Concentration  $\mu\text{g}/\text{m}^3$	Foundation Dimensions (m x m)	Initial Oxygen Concentration (%)	Simulated Transport Time with Biodegradation  Years	Oxygen Shadow?	Minimum Oxygen Concentration Directly Beneath the Slab		Minimum Oxygen Concentration 1 m (3 ft) Beneath the Slab	
					C/Catm	(%)	C/Catm	(%)
Slab-on-grade Building Square Shape (meters x meters)								
10,000	10 x 10	21	0.5	no	0.99	20.8	0.99	20.8
10,000	10 x 10	21	1	no	0.99	20.8	0.99	20.8
10,000	10 x 10	21	9	no	0.99	20.8	0.99	20.8
10,000	10 x 10	21	50	no	0.99	20.8	0.99	20.8
10,000	90 x 90	21	1	no	0.99	20.8	0.99	20.8
10,000	90 x 90	10.5	1	no	0.50	10.4	0.50	10.4
10,000	90 x 90	21	9	no	0.97	20.4	0.97	20.4
10,000	90 x 90	10.5	9	no	0.48	10.1	0.48	10.1
10,000	90 x 90	21	50	no	0.87	18.3	0.87	18.3
10,000	90 x 90	10.5	50	no	0.48	10.1	0.48	10.1
10,000	120 x 120	21	9	no	0.98	20.6	0.98	20.6
10,000	120 x 120	10.5	9	no	0.49	10.2	0.49	10.2
10,000	120 x 120	21	50	no	0.9	18.9	0.9	18.9

**Table B-1. Matrix Summarizing Simulations Run with Source at 5 ft (1.6 m)**

Full Domain Scale (International Units)								
Geology: Homogeneous Sand								
Source Vapor Concentration  $\mu\text{g}/\text{m}^3$	Foundation Dimensions (m x m)	Initial Oxygen Concentration (%)	Simulated Transport Time with Biodegradation  Years	Oxygen Shadow?	Minimum Oxygen Concentration Directly Beneath the Slab		Minimum Oxygen Concentration 1 m (3 ft) Beneath the Slab	
					C/Catm	(%)	C/Catm	(%)
10,000	120 x 120	10.5	50	no	0.44	9.2	0.44	9.2
10,000	240 x 240	21	0.8	no	0.99	20.8	0.99	20.8
10,000	632 x 632	21	9	no	0.99	20.8	0.99	20.8
10,000	632 x 632	21	20	no	0.99	20.7	0.99	20.7
10,000	632 x 632	21	50	no	0.96	20.2	0.96	20.2
10,000	632 x 632	10.5	20	no	0.49	10.2	0.49	10.2
10,000	632 x 632	10.5	50	no	0.46	9.7	0.46	9.7
100,000	10 x 10	21	1	no	0.99	20.8	0.99	20.8
100,000	10 x 10	21	9	no	0.98	20.6	0.98	20.6
100,000	10 x 10	21	50	no	0.98	20.6	0.98	20.6
100,000	90 x 90	21	1	no	0.99	20.7	0.99	20.7
100,000	90 x 90	10.5	1	no	0.48	10.1	0.48	10.1
100,000	90 x 90	21	9	no	0.91	19.2	0.91	19.2
100,000	90 x 90	10.5	9	no	0.42	8.7	0.42	8.7
100,000	90 x 90	21	50	no	0.57	11.9	0.57	11.9
100,000	90 x 90	10.5	50	no	0.17	3.5	0.17	3.5

**Table B-1. Matrix Summarizing Simulations Run with Source at 5 ft (1.6 m)**

Full Domain Scale (International Units)								
Geology: Homogeneous Sand								
Source Vapor Concentration  $\mu\text{g}/\text{m}^3$	Foundation Dimensions (m x m)	Initial Oxygen Concentration (%)	Simulated Transport Time with Biodegradation  Years	Oxygen Shadow?	Minimum Oxygen Concentration Directly Beneath the Slab		Minimum Oxygen Concentration 1 m (3 ft) Beneath the Slab	
					C/Catm	(%)	C/Catm	(%)
100,000	120 x 120	21	9	no	0.92	19.3	0.92	19.3
100,000	120 x 120	10.5	9	no	0.42	8.7	0.42	8.7
100,000	120 x 120	21	50	no	0.58	12.1	0.58	12.1
100,000	120 x 120	10.5	50	no	0.11	2.3	0.11	2.3
100,000	632 x 632	21	9	no	0.93	19.6	0.93	19.6
100,000	632 x 632	21	20	no	0.85	17.9	0.85	17.9
100,000	632 x 632	10.5	20	no	0.35	7.2	0.35	7.2
100,000	632 x 632	21	50	no	0.63	13.2	0.63	13.2
100,000	632 x 632	10.5	50	no	0.12	2.5	0.12	2.5
1,000,000	10 x 10	21	1	no	0.93	19.5	0.92	19.3
1,000,000	10 x 10	21	9	no	0.85	17.8	0.85	17.7
1,000,000	10 x 10	21	50	no	0.85	17.8	0.85	17.7
1,000,000	30 x 30	21	9	no	0.59	12.3	0.58	12.2
1,000,000	40 x 40	21	9	no	0.59	12.4	0.59	12.3
1,000,000	40 x 40	10.5	9	<b>yes</b>	0.05	1.0	0.05	1.0
1,000,000	40 x 40	21	20	<b>yes</b>	0.05	1.0	0.05	1.0

**Table B-1. Matrix Summarizing Simulations Run with Source at 5 ft (1.6 m)**

Full Domain Scale (International Units)								
Geology: Homogeneous Sand								
Source Vapor Concentration  $\mu\text{g}/\text{m}^3$	Foundation Dimensions (m x m)	Initial Oxygen Concentration (%)	Simulated Transport Time with Biodegradation  Years	Oxygen Shadow?	Minimum Oxygen Concentration Directly Beneath the Slab		Minimum Oxygen Concentration 1 m (3 ft) Beneath the Slab	
					C/Catm	(%)	C/Catm	(%)
1,000,000	60 x 60	21	9	yes	0.05	1.0	0.05	1.0
1,000,000	90 x 90	21	1	no	0.93	19.5	0.93	19.5
1,000,000	90 x 90	10.5	1	no	0.16	3.4	0.15	3.2
1,000,000	90 x 90	21	9	yes	0.05	0.9	0.05	0.9
1,000,000	90 x 90	10.5	9	yes	0.04	0.9	0.04	0.9
1,000,000	90 x 90	21	50	yes	0.04	0.9	0.04	0.9
1,000,000	90 x 90	10.5	50	yes	0.04	0.9	0.04	0.9
1,000,000	120 x 120	21	9	yes	0.05	1.0	0.05	1.0
1,000,000	120 x 120	10.5	9	yes	0.04	0.8	0.04	0.8
1,000,000	120 x 120	21	50	yes	0.04	0.8	0.04	0.8
1,000,000	120 x 120	10.5	50	yes	0.04	0.8	0.04	0.8
1,000,000	632 x 632	21	1	no	0.93	19.5	0.92	19.4
1,000,000	632 x 632	21	3.0	no	0.78	16.4	0.78	16.3
1,000,000	632 x 632	10.5	3.0	yes	0.05	1.0	0.05	1.0
1,000,000	632 x 632	21	6.0	no	0.56	11.8	0.56	11.7
1,000,000	632 x 632	10.5	6.0	yes	0.05	1.0	0.05	1.0
1,000,000	632 x 632	21	9	yes	0.05	1.0	0.05	1.0

**Table B-1. Matrix Summarizing Simulations Run with Source at 5 ft (1.6 m)**

Full Domain Scale (International Units)								
Geology: Homogeneous Sand								
Source Vapor Concentration  $\mu\text{g}/\text{m}^3$	Foundation Dimensions (m x m)	Initial Oxygen Concentration (%)	Simulated Transport Time with Biodegradation  Years	Oxygen Shadow?	Minimum Oxygen Concentration Directly Beneath the Slab		Minimum Oxygen Concentration 1 m (3 ft) Beneath the Slab	
					C/Catm	(%)	C/Catm	(%)
2,000,000	10 x 10	21	0.5	no	0.86	18.1	0.85	17.9
5,000,000	10 x 10	21	0.5	no	0.32	6.7	0.29	6.1
5,000,000	120 x 120	21	0.8	yes	0.05	1.0	0.05	1.0
5,000,000	240 x 240	21	0.8	yes	0.05	1.0	0.05	1.0
5,000,000	632 x 632	21	0.8	yes	0.05	1.0	0.05	1.0
10,000,000	10 x 10	21	0.5	yes	0.05	1.0	0.05	1.0
10,000,000	20 x 20	21	0.5	yes (X)	See simulation with dimensions 10 x 10 above			
10,000,000	30 x 30	21	0.5	yes (X)				
10,000,000	90 x 90	21	0.8	yes	0.05	1.0	0.05	1.0
Slab-on-grade Building Rectangular Shape (meters x meters)								
10,000	10 x 90	--	--	no (X)	See simulations with dimensions 90 x 90 above			
10,000	30 x 90	--	--	no (X)				
10,000	60 x 90	--	--	no (X)				

**Table B-1. Matrix Summarizing Simulations Run with Source at 5 ft (1.6 m)**

Full Domain Scale (International Units)								
Geology: Homogeneous Sand								
Source Vapor Concentration  $\mu\text{g}/\text{m}^3$	Foundation Dimensions (m x m)	Initial Oxygen Concentration (%)	Simulated Transport Time with Biodegradation  Years	Oxygen Shadow?	Minimum Oxygen Concentration Directly Beneath the Slab		Minimum Oxygen Concentration 1 m (3 ft) Beneath the Slab	
					C/Catm	(%)	C/Catm	(%)
1,000,000	10 x 632	21	6	no	0.78	16.3	0.77	16.2
1,000,000	10 x 632	21	9	no	0.76	15.9	0.75	15.8
1,000,000	10 x 632	21	20	no	0.75	15.6	0.74	15.5
10,000,000	10 x 90	21	0.8	yes	0.05	1.0	0.05	1.0
10,000,000	20 x 90	21	0.8	yes (X)	See simulation with dimensions 10 x 90 above			
10,000,000	30 x 90	21	0.8	yes (X)				
10,000,000	60 x 90	21	0.8	yes (X)	See simulation with dimensions 10 x 90 above			

(X) means the simulation was not run separately, but the qualitative result was obvious by inspection based on results of other simulations.

**Table B-2. Matrix Summarizing Simulations Run with Source at 15 ft (4.6 m)**

Full Domain Scale (International Units)								
Geology: Homogeneous Sand								
Source Vapor Concentration  µg/m <sup>3</sup>	Foundation Dimensions (m x m)	Initial Oxygen Concentration (%)	Simulated Transport Time with Biodegradation  Years	Oxygen Shadow?	Minimum Oxygen Concentration Directly Beneath the Slab		Minimum Oxygen Concentration 1 m (3 ft) Beneath the Slab	
					C/Catm	(%)	C/Catm	(%)
Slab-on-grade Building Square Shape (meters x meters)								
1,000,000	90 x 90	21	9	no	0.59	12.3	0.58	12.3
1,000,000	90 x 90	10.5	9	yes	0.05	1.0	0.05	1.0
1,000,000	90 x 90	21	20	no	0.23	4.9	0.23	4.8
1,000,000	120 x 120	21	9	no	0.70	14.7	0.70	14.7
1,000,000	120 x 120	21	20	no	0.34	7.1	0.34	7.1
1,000,000	120 x 120	21	50	yes	0.05	1.0	0.05	1.0
1,000,000	200 x 200	10.5	8	no	0.23	4.8	0.22	4.6
1,000,000	200 x 200	21	9	no	0.71	14.9	0.71	14.9
1,000,000	200 x 200	10.5	9	yes	0.05	1.0	0.05	1.0
1,000,000	200 x 200	21	20	no	0.36	7.6	0.36	7.6
1,000,000	200 x 200	10.5	20	yes	0.04	0.9	0.04	0.9
1,000,000	240 x 240	10.5	8	no	0.22	4.6	0.22	4.6
1,000,000	240 x 240	21	9	no	0.71	14.9	0.71	14.9

**Table B-2. Matrix Summarizing Simulations Run with Source at 15 ft (4.6 m)**

Full Domain Scale (International Units)

Geology: Homogeneous Sand

Source Vapor Concentration  $\mu\text{g}/\text{m}^3$	Foundation Dimensions (m x m)	Initial Oxygen Concentration (%)	Simulated Transport Time with Biodegradation  Years	Oxygen Shadow?	Minimum Oxygen Concentration Directly Beneath the Slab		Minimum Oxygen Concentration 1 m (3 ft) Beneath the Slab	
					C/Catm	(%)	C/Catm	(%)
1,000,000	240 x 240	10.5	9	yes	0.05	1.0	0.05	1.0
1,000,000	240 x 240	21	20	no	0.36	7.6	0.35	7.4
1,000,000	632 x 632	21	6	no	0.81	17.0	0.81	17.0
1,000,000	632 x 632	10.5	8	no	0.20	4.2	0.20	4.2
1,000,000	632 x 632	21	9	no	0.71	14.9	0.71	14.9
1,000,000	632 x 632	10.5	9	yes	0.05	1.0	0.05	1.0
1,000,000	632 x 632	21	20	no	0.36	7.6	0.36	7.6
5,000,000	90 x 90	21	9	yes	0.05	0.9	0.05	0.9
10,000,000	10 x 10	21	0.5	no	0.29	6.1	0.28	5.9
10,000,000	10 x 10	21	1	no	0.29	6.1	0.28	5.9
10,000,000	10 x 10	21	9	no	0.29	6.1	0.28	5.9
10,000,000	10 x 10	21	50	no	0.29	6.1	0.28	5.9
10,000,000	10 x 10	10.5	50	no	0.29	6.1	0.28	5.9
10,000,000	20 x 20	21	1	no	0.06	1.3	0.06	1.3



**Table B-2. Matrix Summarizing Simulations Run with Source at 15 ft (4.6 m)**

Full Domain Scale (International Units)								
Geology: Homogeneous Sand								
Source Vapor Concentration  $\mu\text{g}/\text{m}^3$	Foundation Dimensions (m x m)	Initial Oxygen Concentration (%)	Simulated Transport Time with Biodegradation  Years	Oxygen Shadow?	Minimum Oxygen Concentration Directly Beneath the Slab		Minimum Oxygen Concentration 1 m (3 ft) Beneath the Slab	
					C/Catm	(%)	C/Catm	(%)
10,000,000	20 x 20	21	9	no	0.06	1.3	0.06	1.3
10,000,000	20 x 20	21	20	no	0.06	1.3	0.06	1.3
10,000,000	30 x 30	21	0.8	yes	0.05	1.0	0.05	1.0
10,000,000	90 x 90	21	0.8	yes	0.05	1.0	0.05	1.0
10,000,000	90 x 90	21	9	yes	0.04	0.9	0.04	0.9
10,000,000	632 x 632	21	0.05	no	0.42	8.8	0.42	8.8
10,000,000	632 x 632	21	0.08	no	0.14	2.9	0.13	2.7
10,000,000	632 x 632	21	1	yes	0.05	1.0	0.05	1.0
Slab-on-grade Building Rectangular Shape (meters x meters)								
10,000,000	10 x 90	21	0.8	no	0.20	4.1	0.19	3.9
10,000,000	10 x 90	21	9	no	0.19	4.0	0.19	4.0
10,000,000	10 x 90	10.5	20	no	0.19	4.0	0.19	4.0
10,000,000	10 x 90	21	50	no	0.19	4.0	0.19	4.0
10,000,000	20 x 90	21	0.8	yes	0.05	1.0	0.05	1.0
10,000,000	30 x 90	21	0.8	yes	0.05	1.0	0.05	1.0

**Table B-2. Matrix Summarizing Simulations Run with Source at 15 ft (4.6 m)**

**Full Domain Scale (International Units)**

**Geology: Homogeneous Sand**

Source Vapor Concentration  $\mu\text{g}/\text{m}^3$	Foundation Dimensions (m x m)	Initial Oxygen Concentration (%)	Simulated Transport Time with Biodegradation  Years	Oxygen Shadow?	Minimum Oxygen Concentration Directly Beneath the Slab		Minimum Oxygen Concentration 1 m (3 ft) Beneath the Slab	
					C/Catm	(%)	C/Catm	(%)
10,000,000	60 x 90	21	0.8	yes	0.05	1.0	0.05	1.0
10,000,000	10 x 632	21	1	no	0.20	4.1	0.20	4.1
10,000,000	10 x 632	21	6	no	0.20	4.1	0.20	4.1
10,000,000	10 x 632	21	9	no	0.20	4.1	0.20	4.1
10,000,000	10 x 632	21	20	no	0.20	4.1	0.20	4.1

**Table B-3. Matrix Summarizing Simulations Run with Source at 30 ft (9 m)**

Full Domain Scale (International Units)								
Geology: Homogeneous Sand								
Source Vapor Concentration  $\mu\text{g}/\text{m}^3$	Foundation Dimensions (m x m)	Initial Oxygen Concentration (%)	Simulated Transport Time with Biodegradation  Years	Oxygen Shadow?	Minimum Oxygen Concentration Directly Beneath the Slab		Minimum Oxygen Concentration 1 m (3 ft) Beneath the Slab	
					C/Catm	(%)	C/Catm	(%)
<b>Slab-on-grade Building Square Shape (meters x meters)</b>								
10,000,000	30 x 30	21	1	no	0.14	2.9	0.14	2.9
10,000,000	30 x 30	21	6	no	0.14	2.9	0.14	2.9
10,000,000	30 x 30	21	9	no	0.14	2.9	0.14	2.9
10,000,000	30 x 30	21	20	no	0.14	2.9	0.14	2.9
10,000,000	40 x 40	21	1	no	0.062	1.3	0.06	1.3
10,000,000	40 x 40	21	9	no	0.062	1.3	0.06	1.3
10,000,000	40 x 40	21	20	no	0.062	1.3	0.06	1.3
10,000,000	60 x 60	21	1	no	0.06	1.3	0.06	1.3
10,000,000	60 x 60	21	9	no	0.06	1.3	0.06	1.3
<b>Slab-on-grade Building Rectangular Shape (meters x meters)</b>								
10,000,000	10 x 632	21	1	no	0.47	9.9	0.46	9.7
10,000,000	10 x 632	21	6	no	0.47	9.9	0.46	9.7

**Table B-4. Matrix Summarizing Simulations Run with a Silty Clay Layer on Ground Surface**

Full Domain Scale (International Units)

Geology: silty clay on top (1 m thick) and Sand Below

Source Vapor Concentration $\mu\text{g}/\text{m}^3$	Source Depth (m)	Foundation Dimensions (m x m)	Initial Oxygen Concentration (%)	Simulated Transport Time with Biodegradation  Years	Oxygen shadow?	Minimum Oxygen Concentration Directly Beneath the Slab		Minimum Oxygen Concentration 1 m (3 ft) Beneath the Slab	
						C/Catm	(%)	C/Catm	(%)
<b>Slab-on-grade Building Square Shape (meters x meters)</b>									
100,000	1.6	632 x 632	21	9	no	0.47	9.9	0.47	9.9
100,000	1.6	632 x 632	21	20	yes	0.049	1.0	0.05	1.0
1,000,000	1.6	30 x 30	21	1	no	0.44	9.2	0.44	9.2
1,000,000	1.6	30 x 30	21	9	yes	0.05	1.0	0.05	1.0
1,000,000	1.6	40 x 40	21	1	no	0.32	6.7	0.32	6.7
1,000,000	1.6	40 x 40	21	9	yes	0.05	1.0	0.05	1.0
1,000,000	4.6	120 x 120	21	4	no	0.24	5.0	0.24	5.0
1,000,000	4.6	120 x 120	21	9	yes	0.05	1.0	0.05	1.0
1,000,000	4.6	200 x 200	21	4	no	0.24	5.0	0.24	5.0
1,000,000	4.6	200 x 200	21	9	yes	0.05	1.0	0.05	1.0
1,000,000	4.6	240 x 240	21	4	no	0.24	5.0	0.24	5.0
1,000,000	4.6	240 x 240	21	9	yes	0.05	1.0	0.05	1.0

**Table B-4. Matrix Summarizing Simulations Run with a Silty Clay Layer on Ground Surface**

**Full Domain Scale (International Units)**

**Geology: silty clay on top (1 m thick) and Sand Below**

Source Vapor Concentration $\mu\text{g}/\text{m}^3$	Source Depth (m)	Foundation Dimensions (m x m)	Initial Oxygen Concentration (%)	Simulated Transport Time with Biodegradation  Years	Oxygen shadow?	Minimum Oxygen Concentration Directly Beneath the Slab		Minimum Oxygen Concentration 1 m (3 ft) Beneath the Slab	
						C/Catm	(%)	C/Catm	(%)
10,000,000	4.6	632 x 632	21	4	no	0.24	5.0	0.24	5.0
10,000,000	9	30 x 30	21	6	no	0.09	1.9	0.09	1.9
10,000,000	9	30 x 30	21	9	no	0.09	1.9	0.09	1.9
10,000,000	9	40 x 40	21	6	yes	0.05	1.0	0.05	1.0
<b>Slab-on-grade Building Rectangular Shape (meters x meters)</b>									
1,000,000	1.6	10 x 632	21	1	no	0.66	13.9	0.65	13.7
1,000,000	1.6	10 x 632	21	9	no	0.53	11.1	0.52	10.9
1,000,000	1.6	10 x 632	21	20	no	0.52	10.9	0.52	10.9
10,000,000	4.6	10 x 60	21	1	no	0.10	2.1	0.10	2.0
10,000,000	4.6	10 x 60	21	9	no	0.10	2.1	0.10	2.0
10,000,000	4.6	10 x 60	21	20	no	0.10	2.1	0.10	2.0
10,000,000	4.6	10 x 90	21	1	no	0.10	2.1	0.10	2.0
10,000,000	4.6	10 x 90	21	9	no	0.10	2.1	0.10	2.0
10,000,000	4.6	10 x 632	21	1	no	0.10	2.1	0.10	2.0
10,000,000	4.6	10 x 632	21	6	no	0.10	2.1	0.10	2.0

**Table B-4. Matrix Summarizing Simulations Run with a Silty Clay Layer on Ground Surface**

Full Domain Scale (International Units)

Geology: silty clay on top (1 m thick) and Sand Below

Source Vapor Concentration $\mu\text{g}/\text{m}^3$	Source Depth (m)	Foundation Dimensions (m x m)	Initial Oxygen Concentration (%)	Simulated Transport Time with Biodegradation  Years	Oxygen shadow?	Minimum Oxygen Concentration Directly Beneath the Slab		Minimum Oxygen Concentration 1 m (3 ft) Beneath the Slab	
						C/Catm	(%)	C/Catm	(%)
10,000,000	4.6	10 x 632	21	9	no	0.10	2.1	0.10	2.0
10,000,000	9	10 x 632	21	1	no	0.33	6.9	0.33	6.9
10,000,000	9	10 x 632	21	9	no	0.33	6.9	0.33	6.9

**Table B-5. Matrix Summarizing Simulations Run with Source at 5 ft (1.6 m) Below a Basement**

Full Domain Scale (International Units)								
Geology: Homogeneous Sand								
Building With Full Basement Square Shape (meters x meters) Basement Depth of 2 m bgs								
Source Vapor Concentration  $\mu\text{g}/\text{m}^3$	Foundation Dimensions (m x m)	Initial Oxygen Concentration (%)	Simulated Transport Time with Biodegradation  Years	Oxygen shadow?	Minimum Oxygen Concentration Directly Beneath the Slab		Minimum Oxygen Concentration 1 m (3 ft) Beneath the Slab	
					C/Catm	(%)	C/Catm	(%)
10,000	632 x 632	21	9	no	0.99	20.8	0.99	20.8
100,000	632 x 632	21	9	no	0.88	18.4	0.88	18.4
1,000,000	632 x 632	21	1.0	no	0.87	18.2	0.86	18.0
1,000,000	632 x 632	21	3.0	no	0.60	12.5	0.59	12.4
1,000,000	632 x 632	21	9	<b>yes</b>	0.05	1.0	0.05	1.0